AEROSPACE REPORT NO.
ATR-2005(5138)-1

Trajectory Reconstruction and Heating Analysis of *Columbia* Composite Debris Pieces

15 April 2005

Prepared by

W. P. HALLMAN and D. M. MOODY
Flight Mechanics Department
Vehicle Systems Division

Prepared for

VOLPE NATIONAL TRANSPORTATION SYSTEMS CENTER
U.S. DEPARTMENT OF TRANPORTATION
Cambridge, MA 02142

Contract No. DTRS57-99-D-00062
Task 9.0

Space Launch Operations

PUBLIC RELEASE AUTHORIZED

THE AEROSPACE CORPORATION
EL SEGUNDO, CALIFORNIA

Technical Report Documentation Page

1. Report No. DOT-VNTSC-FAA-05-03	**2. Government Accession No.**	**3. Recipient's Catalog No.**
4. Title and Subtitle Trajectory Reconstruction and Heating Analysis of *Columbia* Composite Debris Pieces		**5. Report Date** 15 April 2005 **6. Performing Organization Code** DOT-RITA-VNTSC-DTS-67
7. Author(s)* W. P. Hallman and D.M. Moody		**8. Performing Organization Report No.** ATR-2005(5138)-1
9. Performing Organization Name and Address U.S. Department of Transportation Research and Innovative Technology Administration Volpe National Transportation Systems Center Aviation Safety Division Cambridge, MA 02142-1093		**10. Work Units No. (TRAIS)** FA-2R, BL411 **11. Contract or Grant No.**
12. Sponsoring Agency Name and Address U.S. Department of Transportation Federal Aviation Administration Office of the Assoc. Administrator for Commercial Space Transportation Washington, DC 20591		**13. Type of Report and Period Covered** **14. Sponsoring Agency Code** FAA/AST-300

15. Supplementary Notes

*The Aerospace Corporation, El Segundo, CA 90245-4691, under contract to the Volpe National Transportation Systems Center -- DTRS57-99-D-00062, Task 9.0

Aerospace Corporation Report No. ATR-2005(5138)-1

16. Abstract

The Aerospace Corporation was tasked by the Volpe National Transportation Systems Center to provide technical support to the Federal Aviation Administration, Office of Commercial Space Transportation (FAA/AST), to develop reentry trajectory profiles and heating estimates for selected composite material debris pieces recovered following the *Columbia* accident. A list of eight composite debris items were requested from NASA, and subsequently delivered to The Aerospace Corporation. These eight pieces consisted of three odd-shaped fragments, four gaseous tanks, and a single irregularly shaped portion of the payload bay door. After delivery of the *Columbia* composite material debris pieces, each object was weighed and its dimensions determined. With this information, drag coefficients for each debris piece were estimated for different reentry configurations (tumbling or broadside.) A *Columbia* reentry trajectory simulation developed at The Aerospace Corporation was then used to define plausible reentry trajectories for each debris piece assuming different breakup scenarios. The trajectory profile for each debris piece was initialized at a point on a reconstructed *Columbia* reentry trajectory. The time when the debris piece emanated from this primary trajectory was varied in each case. Optimization techniques were then used to vary the independent variables so that the impact location of the debris piece landed exactly, or close to, the observed impact location. Results from this analysis show that the initial breakup times varied by 60 seconds across all of the cases considered. Based on these reentry trajectories, estimates were obtained for heating rate, total heating, aerodynamic loads and dynamic pressure experienced by each recovered item. A new composite material ablation model was developed and used to predict the mass loss from the exposed rib structure of the payload bay door debris piece. The predicted mass loss is shown to closely agree with the observed value determined from laboratory analysis.

17. Key Words Trajectory reconstruction, reentry simulation, drag estimation, optimization, reentry heating, ablation		**18. Distribution Statement** PUBLIC RELEASE AUTHORIZED	
19. Security Classification. (of this report) None	**20. Security Classification. (of this page)** None	**21. No. of Pages** 63	**22. Price**

Form DOT F 1700.7 (8-72) **Reproduction of completed page authorized**

AEROSPACE REPORT NO.
ATR-2005 (5138)-1

TRAJECTORY RECONSTRUCTION AND HEATING ANALYSIS OF *COLUMBIA* COMPOSITE DEBRIS PIECES

Prepared by

W. P. HALLMAN AND D. M. MOODY
Flight Mechanics Department
Vehicle Systems Division

15 April 2005

Space Program Operations
THE AEROSPACE CORPORATION
El Segundo, CA 90245

Prepared for

VOLPE NATIONAL TRANSPORTATION SYSTEMS CENTER
U.S. DEPARTMENT OF TRANPORTATION
Cambridge, MA 02142

Contract No. DTRS57-99-D-00062
Task 9.0

PUBLIC RELEASE AUTHORIZED

AEROSPACE REPORT NO.
ATR-2005 (5138)-1

TRAJECTORY RECONSTRUCTION AND HEATING ANALYSIS OF *COLUMBIA* COMPOSITE DEBRIS PIECES

Prepared by

W. P. HALLMAN
Flight Mechanics Department
Vehicle Systems Division

D. M. MOODY
Flight Mechanics Department
Vehicle Systems Division

Approved by:

E. K. RUTH, Systems Director
Commercial Launch Systems
Space Launch Support Division

Abstract

The Aerospace Corporation was tasked by the Volpe National Transportation Systems Center to provide technical support to the Federal Aviation Administration, Office of Commercial Space Transportation (FAA/AST), to develop reentry trajectory profiles for selected composite material debris pieces recovered following the *Columbia* accident. A list of eight composite debris items were requested from NASA and subsequently delivered to The Aerospace Corporation. These eight pieces consisted of three odd-shaped fragments, four gaseous tanks, and a single irregularly shaped portion of the payload bay door. After delivery of the *Columbia* composite material debris pieces, each object was weighed and its dimensions determined. With this information, drag coefficients for each debris piece were estimated for different reentry configurations (tumbling or broadside.) A *Columbia* reentry trajectory simulation developed at The Aerospace Corporation was then used to define plausible reentry trajectories for each debris piece assuming different breakup scenarios. The trajectory profile for each debris piece was initialized at a point on a reconstructed *Columbia* reentry trajectory. The time when the debris piece emanated from this primary trajectory was varied in each case. The four breakup scenarios considered were:

1. Single breakup with an instantaneous delta-v at breakup.
2. Single breakup with lift force
3. Double breakup with larger intermediate debris object
4. Single breakup with instantaneous delta-v and delta-x at breakup

Optimization techniques were then used to vary the independent variables so that the impact location of the debris piece landed exactly, or close to, the observed impact location. Results from this analysis show that the initial breakup times varied by 60 seconds across all of the cases considered. Based on these reentry trajectories, estimates were obtained for heating rate, total heating, aerodynamic loads and dynamic pressure experienced by each recovered item. A new composite material ablation model was developed and used to predict the mass loss from the exposed rib structure of the payload bay door debris piece. The predicted mass loss is shown to closely agree with the observed value determined from laboratory analysis.

Acknowledgments

Dr. Wayne P. Hallman and Robert W. Seibold served as Principal Investigator and Program Manager, respectively. Dr. Douglas M. Moody was co-investigator and co-author of the final report. The authors wish to thank Dr. Richard L. Baker for his help in developing a simplified composite material ablation model. The authors are grateful for the valuable support of Dr. Gary L. Steckel, who performed laboratory analysis of the payload bay door debris piece, under Air Force Space and Missile Systems Center funding provided to The Aerospace Corporation. The authors also thank Dr. William H. Ailor for his insight and valuable guidance.

Gratitude is extended to Mr. Lyndon Bonaparte at the Office of the Associate Administrator for Commercial Space Transportation, Federal Aviation Administration, for valuable guidance on FAA/AST regulatory and licensing needs. The authors also wish to thank Mr. John J. Sigona, who served as the Contracting Officer's Technical Representative (COTR) at the Volpe National Transportation Systems Center and provided valuable insight on government needs and regulations.

Contents

1. INTRODUCTION 1

2. AERODYNAMIC DRAG ESTIMATES FOR DEBRIS PIECES 3

2.1 WEIGHTS, DIMENSIONS, AND REFERENCE AREAS 4
2.1.1 Reference Areas for the COPVs 4
2.1.2 Reference Area for the Payload Bay Door Fragment 4
2.2 DRAG COEFFICIENTS IN FREE-MOLECULAR AND HYPERSONIC CONTINUUM FLOW ... 5
2.2.1 Drag Coefficients for the COPVs 5
2.2.2 Drag Coefficients for the Payload Bay Door Fragment 5
2.3 DRAG COEFFICIENT DEPENDENCE ON KNUDSEN NUMBER AND MACH NUMBER 5

3. TRAJECTORY RECONSTRUCTION PROCESS 7

3.1 DATA SOURCES 7
3.2 DEBRIS TRAJECTORY SIMULATION 8
3.2.1 Method #1: Instantaneous Delta-V 9
3.2.2 Method #2: Directional Lift Force 9
3.2.3 Method #3: Secondary Breakup 9
3.2.4 Method #4: Instantaneous Delta-V and Delta-X 9

4. RESULTS 11

4.1 DEBRIS #1 13
4.2 DEBRIS #2 13
4.3 DEBRIS #3 14
4.4 DEBRIS #4 14
4.5 DEBRIS #5 14
4.6 DATA ANALYSIS 15

5. SIMPLIFIED COMPOSITE HEATING MODEL 19

6. ABLATION MODEL PREDICTIONS FOR PAYLOAD BAY DOOR RIB STRUCTURE 23

7. CONCLUSIONS 25

8. ABBREVIATIONS AND SYMBOLS 55

9. REFERENCES 57

Figures

Figure 1: Payload Bay Door # 53993 27
Figure 2: MPS/OMS Kevlar Helium Tank # 1119 28
Figure 3: RCS Helium Tank # 38913 29
Figure 4: Kevlar Wound Tank #49386 30
Figure 5: Kevlar Wound Tank # 147 31
Figure 6: Wind Profile Along Debris #5 Reentry Trajectory 32
Figure 7: C_d vs Mach Number for Debris #5 33
Figure 8: Impact Locations and Debris Pictures 34
Figure 9: *Columbia* Debris Footprint and Composite Debris Impact Locations 35
Figure 10: Reentry Heating and Loads Data for Debris #1 Random Tumbling Aerodynamics - Method 1 36
Figure 11: Reentry Altitude and Velocity Data for Debris #1 Random Tumbling Aerodynamics - Method 1 37
Figure 12: Reentry Heating and Loads Data for Debris #1 Trimmed Aerodynamics - Method 1 38
Figure 13: Reentry Altitude and Velocity Data for Debris #1 Trimmed Aerodynamics - Method 1 39
Figure 14: Reentry Heating and Loads Data for Debris #2 Method 4 40
Figure 15: Reentry Altitude and Velocity Data for Debris #2 Method 4 41
Figure 16: Reentry Heating and Loads Data for Debris #3 Method 4 42
Figure 17: Reentry Altitude and Velocity Data for Debris #3 Method 4 43
Figure 18: Reentry Heating and Loads Data for Debris #4 Method 4 44
Figure 19: Reentry Altitude and Velocity Data for Debris #4 Method 4 45
Figure 20: Reentry Heating and Loads Data for Debris #5 Method 4 46
Figure 21: Reentry Altitude and Velocity Data for Debris #5 Method 4 47
Figure 22: Enthalpy of Air 48
Figure 24: Payload Bay Door Sample Areas for Laboratory Analysis 50
Figure 25: Predicted Wall Temperature for Payload Bay Door Area 4 with k_2 Varied 51
Figure 26: Predicted Cumulative Mass Loss for Payload Bay Door Area 4 with k_2 Varied... 52
Figure 27: Predicted Payload Bay Door Area 4 Total Mass Loss with k_2 Varied 53

Tables

Table 1: Debris Items and Impact Location 3
Table 2: Description of Debris Items 4
Table 3: Summary of Trajectory Reconstructions 12
Table 4: Summary of Trajectory Reconstructions for Debris # 1 16
Table 5: Summary of Trajectory Reconstructions for Debris # 2 16
Table 6: Summary of Trajectory Reconstructions for Debris # 3 17
Table 7: Summary of Trajectory Reconstructions for Debris # 4 17
Table 8: Summary of Trajectory Reconstructions for Debris # 5 18

1. INTRODUCTION

Tools used to predict hazards to people and property from reentering launch and spacecraft hardware rely on models of how the materials used in building space hardware are expected to respond to the heating and loads environment. In some cases, models have been calibrated based on material that is found on the ground after a reentry ends. For example, several 570 lb stainless steel tanks from Delta II second stages have been recovered. Post reentry trajectory and laboratory analyses of these nearly intact tanks have been invaluable in helping calibrate reentry heating models. Numerous instances of spacecraft titanium tanks surviving reentry have also helped validate reentry heating model predictions. Debris recovered following the *Columbia* accident provides a unique opportunity to further understand the reentry breakup process and component survivability. *Columbia* debris items containing composite materials are of particular interest. Prior to the *Columbia* accident, there were no documented cases where composite material items not designed to ablate had been recovered from a reentering stage or spacecraft. The Space Shuttle Orbiters have composite materials in a number of locations, including reinforced-carbon-carbon (RCC) on the wing leading edges, graphite/epoxy payload bay doors, graphite/epoxy skin on the Orbital-Maneuvering-System pods and composite over-wrapped pressure vessels (COPVs). While the RCC structure is designed to survive stagnation heating rates on reentry, the other composite materials are not, and thus are of primary interest.

The primary objective of this study is to further our understanding of composite material reentry survivability. To this end, eight composite *Columbia* debris items were requested from NASA, and subsequently delivered to The Aerospace Corporation. These eight pieces consisted of three odd-shaped fragments, four gaseous tanks, and a single irregularly shaped portion of the payload bay door. The first step in developing reentry trajectory profiles for these items was to estimate their aerodynamic characteristics. Based on each object's weight and dimensions, drag coefficients for each debris piece were estimated. For irregularly shaped pieces, both trimmed and tumbling attitudes were considered. A *Columbia* reentry trajectory simulation developed at The Aerospace Corporation was then used to define plausible reentry trajectories for each debris piece assuming different breakup scenarios. From these trajectory reconstructions, estimates for heating rate, total heating, and aerodynamic loads experienced by each recovered item were determined. This report also includes a description of a simplified composite material ablation model. This model was applied to the payload bay door debris piece, and the predicted mass loss from this model is compared to estimates obtained from laboratory analysis.

2. AERODYNAMIC DRAG ESTIMATES FOR DEBRIS PIECES

In July of 2004, eight pieces of debris from the wreckage of the Space Shuttle Orbiter *Columbia* were shipped to The Aerospace Corporation from Kennedy Space Center. Four of the pieces are composite over-wrapped pressure vessels (COPVs) which are spherical in shape. The fifth piece, a portion of the payload bay door, is irregular in shape. The final three pieces are fragments of the graphite/epoxy skin from the Orbital-Maneuvering-System (OMS) pods. This section of the report documents the calculation of reference area and drag coefficient for the COPVs and payload door pieces. These numbers were calculated for use in simulating the ballistic descent trajectories of these pieces. A description of each item and an object number used in this report is contained in Table 1. Pictures of the five debris objects analyzed in this report are contained in Figures 1 to 5.

Table 1: Debris Items and Impact Location

Piece No.	KSC ID	Field Description	Engineering Description	Impact Latitude (deg)	Impact Longitude (deg)
1	53993	Payload Bay Door	PLBD	31.838	-95.3874
2	1119	COPV (40 - inch)	MPS/OMS 17.3 cu. Ft. Kevlar Helium Tank	31.3464	-93.9837
3	38913	COPV (18 - inch)	Aft RCS Helium Fuel or Ox, LP05 or RP05	31.4751	-94.3916
4	49386	COPV (26 – inch)	MPS Ghe Aft Tank (4.7 cu. Ft.)	31.4168	-94.1413
5	147	COPV (26 – inch)	ECLSS/PRSD 4.7 cu/. Ft. Kevlar Tank	31.561	-94.476
6	62090	PLBD Composite	OMS POD	31.9434	-95.706
7	62414	PLBD w/FRSI	OMS POD Section	31.9036	-95.7122
8	62622	Honeycomb & Composite Pieces	Honeycomb/Carbon Fiber Skin, Suspect OMS POD	32.0187	-95.9132

2.1 Weights, Dimensions, and Reference Areas

The following table lists the pieces, their shape, weight, computed aerodynamic reference area, and a body length, *L*, to be used in computing Knudsen numbers for the piece.

Table 2: Description of Debris Items

Piece No.	KSC Ident	Description	Shape	Weight (lb)	A_{ref} (ft^2)	L (ft)
1	53993	Payload Bay Door	irregular	46	8.6200	2.930
2	1119	COPV (40 - inch)	sphere	262	7.9253	3.167
3	38913	COPV (18 - inch)	sphere	26	1.8069	1.500
4	49386	COPV (26 - inch)	sphere	72	3.1912	2.000
5	147	COPV (26 - inch)	sphere	53	3.1841	2.000

2.1.1 Reference Areas for the COPVs

The diameter of the largest COPV (piece #2) is 38 inches. The diameter of the smallest (piece #3) is 18 inches. The diameter of each of the intermediate-sized COPVs (pieces #4 and #5) is 24 inches. For these four spherical COPVs the body length was taken as the sphere diameter. The reference area for each was computed as πr^2 plus the mean of the maximum cross-sectional area of the pressure fittings remaining on these vessels.

2.1.2 Reference Area for the Payload Bay Door Fragment

For the irregularly-shaped payload bay door fragment, the projected area in each of three orthogonal views was first computed. The first view (denoted as the x-axis view) is a view from the interior of the payload bay, looking radially outward (normal to the longitudinal, or y-axis of the Orbiter.) From measuring the dimensions of this surviving fragment of the door, it was found that

$$A_x = 15.89 \text{ ft}^2$$

The next view (denoted as the y-axis view) is edge-on, along the longitudinal, or y-axis. Measuring the dimensions in this view gave

$$A_y = 2.90 \text{ ft}^2$$

Measuring dimensions in the z-axis view (orthogonal to both the above views) gave

$$A_z = 8.62 \text{ ft}^2$$

Because of the non-uniform weight distribution of this fragment, it appeared that this door fragment may possibly have trimmed along its z-axis during free fall. For this reason, A_z was chosen as the reference area for this piece. The characteristic body length, *L*, was chosen as the square root of A_z (2.93 ft.)

2.2 Drag Coefficients in Free-Molecular and Hypersonic Continuum Flow

For each piece, a drag coefficient is desired for both the free-molecular (FM) and the hypersonic continuum (HC) flow regimes.

2.2.1 Drag Coefficients for the COPVs

The drag coefficient for a sphere has the following values in the two flow regimes.

$$C_{D,FM} = 2.06 \quad \text{and} \quad C_{D,HC} = 0.92$$

2.2.2 Drag Coefficients for the Payload Bay Door Fragment

The payload bay door fragment was treated as a rectangular box with faces of area A_x, A_y, and A_z. If, as it fell, the box were to trim to A_z (selected as the reference area for drag) then the corresponding drag coefficients in the two flow regimes would be those for a flat plate with the air stream normally incident:

$$C_{D,FM} = 2.06 \quad \text{and} \quad C_{D,HC} = 1.84$$

On the other hand, if the box were to randomly tumble during its fall, the drag coefficients would involve an averaging of the face areas. Specifically, in the free molecular regime we would have

$$C_{D,FM} = 2.06 \frac{A_x + A_y + A_z}{2A_z} = 3.275$$

and in the hypersonic continuum regime we would have

$$C_{D,HC} = 1.84 \frac{A_x + A_y + A_z}{4A_z} = 1.463$$

2.3 Drag Coefficient Dependence on Knudsen Number and Mach Number

At each altitude in a simulation, a Knudsen number for the flow past a bluff body may be computed as a function of the density at altitude and the characteristic body length.

$$Kn = \frac{\lambda_0 \, \rho_0}{L \, \rho}$$

The numerator on the right-hand side (product of the sea-level values of mean free path and density) has the following constant value.

$$\lambda_0 \, \rho_0 = 5.1727 \text{ x } 10^{-10} \quad \text{slug/ft}^2$$

For arbitrary altitude (and thus density) the drag coefficient may be bridged between the free-molecular and hypersonic continuum values as follows.

$$C_{D,1} = \frac{C_{D,HC} + Kn \; C_{D,FM}}{1 + Kn}$$

If we are solidly in the continuum ($Kn < 0.3$) and the Mach number drops below 4.5, then a transonic drag rise may be accounted for by computing a factor, $C_{D,2}$, defined as the following function of Mach number, *M*.

For $M > 4.5$: $\quad C_{D,2} = 1$

For $1.5 < M \le 4.5$: $\quad C_{D,2} = \left[1 + 4x(x^2 - 4.5x)/675\right] / \; 0.92 \quad$ with $\quad x = M - 1.5$

For $0.3 \le M \le 1.5$: $\quad C_{D,2} = \left[0.48 - 520x(x^2 - 1.8x)/864\right] / \; 0.92 \quad$ with $\quad x = M - 0.3$

For $M < 0.3$: $\quad C_{D,2} = 0.48 / 0.92$

Then the final value of drag coefficient as a function of Knudsen number and Mach number is computed as the following product.

$$C_D = C_{D,1} \, C_{D,2}$$

3. TRAJECTORY RECONSTRUCTION PROCESS

3.1 Data Sources

The trajectory reconstruction methodology used to define plausible reentry trajectory profiles for each of the composite debris objects is described in this section. Several different data sources were utilized for this analysis. In Ref. [1], trajectory analysis based on videos and photographs of early debris emanating from *Columbia* is described. This analysis, conducted by The Aerospace Corporation in conjunction with NASA-JSC, investigated small debris objects that were observed breaking off the Orbiter as it flew over California, Nevada and Utah. As part of this study, NASA provided The Aerospace Corporation with highly accurate GPS tracking data of *Columbia* as it reentered. This data ended at approximately 50370 seconds GMT on February 1, 2003 as the Orbiter was passing over central Texas. This loss of signal preceded the main body breakup which occurred at approximately 50421 sec GMT, Ref. [2]. Prior to the main body breakup, portions of the left wing and other externally exposed parts of the Orbiter were known to have broken free of the Orbiter. However, as the following analysis will show, none of the five composite debris objects analyzed in this report could have separated from the Orbiter prior to main body breakup.

Since the GPS derived state vector data ended 50 seconds prior to main body breakup, another data source was required to perform trajectory reconstruction of the debris pieces analyzed in this report. An Aerospace Corporation reconstruction of the *Columbia* reentry trajectory based on sensor data was developed shortly after the *Columbia* accident. This reconstructed trajectory provides complete state vector estimates of *Columbia*'s position and velocity from 47730 sec to 50499 sec GMT. Following main body breakup, this trajectory tracks leading objects from the debris cloud. All trajectory analysis in this report is based on this Aerospace derived reentry trajectory.

As part of the early sighting analysis described in Ref. [1], NASA provided The Aerospace Corporation with atmosphere density and local wind data along *Columbia*'s reentry path. The final version of the atmosphere data is from the Revision D Data Assimilation Office (DAO) model. This model provides density and wind direction/velocity data from ground to an altitude of 250,000 feet as a function of latitude/longitude values along the *Columbia* reentry trajectory. Winds can have a significant effect on reentry trajectory dynamics, especially the final impact location. This effect is more pronounced for low ballistic coefficient items. For example, winds blew a low ballistic coefficient fragment from the Delta II Stage 2 reentry over Texas 30 nm cross track. A sample wind profile for a Debris #5 reentry trajectory is shown in Figure 6. All reentry trajectory simulations performed for this report utilized this NASA atmosphere and wind model.

To model the aerodynamic forces on the debris objects, the drag coefficient data presented in Section 2 was utilized. The weight and aerodynamic reference area data from Table 2 describe the physical properties of the debris. Reentry simulations for the payload door

fragment were performed using both tumbling and trimmed drag coefficients, while for the COPV pieces tumbling drag coefficients were used. The results presented below will show that initial conditions for all debris pieces were in the continuum flow regime with initial velocities corresponding to approximately Mach 15. Thus, the free molecular flow drag coefficient calculations described in Section 2 were not used. As each debris piece reentered, the transonic and subsonic drag coefficient changes described in Section 2 were modeled. A sample drag profile for a Debris #5 reentry trajectory is shown in Figure 7.

The final data source for the reentry reconstruction analysis is the known impact locations of the debris. This information was obtained from the NASA's *Columbia* Reconstruction Database (CRD). This database also contains an engineering description of each debris item. Table 1 contains details of the composite debris analyzed, including the impact locations.

The impact locations along with pictures of the eight debris items are shown in Figure 8. The debris footprint from these items stretches approximately 120 nm in length. In Figure 9, an ellipse encompassing nearly all of the recovered *Columbia* debris is illustrated with the eight composite debris item impact locations. The main body breakup location at 50421 GMT seconds is also noted on this figure. Debris that is uprange of the main body breakup is mostly from the left wing where the initial breach of the Orbiter occurred. The trajectory reconstruction analysis presented below will show that the Debris #1 to #5 did not separate from the Orbiter until after main body breakup.

3.2 Debris Trajectory Simulation

Using the above data sources, trajectory simulations were developed that model the aerodynamic and gravity forces experienced by the debris objects as they reentered. Aerospace's Trajectory Optimization Program (TOP), Ref. [3], was used to simulate the trajectories. The TOP simulations provide a complete time history of the debris object's position and velocity. The debris pieces were all assumed to emanate from the Aerospace Corporation reconstructed *Columbia* reentry profile at an appropriately selected breakup time.

One of the difficulties in estimating debris reentry trajectories is that initial conditions and breakup sequence are not precisely known. The Aerospace Corporation reentry trajectory past main body breakup only approximates the state for a lead object in the debris stream. If the breakup is complex with secondary and other subsequent breakups, the reentry dynamics become extremely difficult to model. For these reasons, four different methods were utilized to simulate reentry trajectory profiles after the debris object separated from the Orbiter until ground impact. These methods should identify a range of plausible reentry trajectory profiles for each piece. All of these methods used an iterative optimization technique to vary independent parameters while satisfying constraints to minimize an objective function. After the optimization process converges, each method defines a unique reentry trajectory profile. Every method varied the initial breakup time when the debris object separated from the *Columbia* reentry trajectory. The four methods are described below.

3.2.1 Method #1: Instantaneous Delta-V

The first method modeled an instantaneous change in the inertial velocity vector (delta-V) at breakup. The three components of the velocity vector were treated as independent parameters that were varied in the optimization process. The source of this delta-V could either be attributed to an explosive breakup, or an initial uncertainty in the object's velocity. The debris object's geodetic latitude and longitude at impact were constrained to match the known impact locations shown in Table 1. The magnitude of the delta-V increment was minimized during the optimization process.

3.2.2 Method #2: Directional Lift Force

The second method modeled a lift force during reentry for the debris object. The ratio of lift to drag (L/D) was treated as an independent parameter along with the lift direction (measured as an Euler roll angle in a relative velocity frame). Both of these parameters were held constant during the debris object's reentry. It is highly unlikely that the lift direction would remain constant during the entire reentry. It is more likely that any lift force would vary in direction due to vehicle tumbling. There are circumstances where a flat plate can auto-rotate about an axis and generate lift in a relatively constant direction. It is also physically possible that a spinning sphere, like the COPVs, can generate lift in a fixed direction if the spin rate is sufficiently high, Ref. [4]. (It was estimated that a spin rate of approximately three revolutions per second about an axis normal to the sphere's velocity would supply the lift required to generate the observed cross track displacement for one of the COPVs.) The debris object's geodetic latitude and longitude at impact were constrained to match the known impact locations shown in Table 1. The magnitude of the lift-to-drag value was minimized during the optimization process.

3.2.3 Method #3: Secondary Breakup

The third method modeled a secondary breakup for the debris object. In this case, after the initial breakup, the drag force for an assumed larger debris object containing the primary object was treated as an optimization parameter. The time of a secondary breakup where the debris piece separates from the larger object and reenters on its own was an optimization parameter. Using this third method, it was not always possible to vary the two breakup times and intermediate ballistic coefficient to cause the debris objects to impact at the exact impact locations. Thus for method #3, an objective function which measured the miss distance on the ground between the simulated debris object impact location and the known impact location was minimized. No optimization constraints were required for this third method.

3.2.4 Method #4: Instantaneous Delta-V and Delta-X

The fourth method modeled an instantaneous change in the inertial velocity vector (delta-V) and inertial position vector (delta-X) at breakup. The three components of the delta velocity vector and the three components of the delta position vector were treated as independent parameters that were varied in the optimization process. The source of this delta-V could either be attributed to an explosive breakup, or an initial uncertainty in the object's velocity

vector. The source of the delta-X vector could be attributed to an initial uncertainty in the object's position. The debris object's geodetic latitude and longitude at impact were constrained to match the known impact locations shown in Table 1. The objective function minimized during the optimization process was chosen to weight the magnitudes of the delta-V and delta-X vectors as

$$F = \Delta V + 0.001\ \Delta X$$

where ΔV is the delta-v magnitude, and ΔX is the delta position magnitude. The weighting factor of 0.001 was chosen after some experimentation to balance the magnitudes of the two vectors.

4. RESULTS

The trajectory reconstruction results for all debris pieces and reconstruction methods are summarized in Table 3. A key to the columns in this table is provided below.

Method	Reconstruction method
Configuration	Random or tumbling aerodynamics
Piece	Debris object number
Impact Error	Distance in feet between reconstructed impact location and actual impact location
Bu_time1	Initial breakup time for debris object
DV Mag	Magnitude of the delta velocity vector at separation
L/D	Magnitude of the lift-to-drag value
Roll Angle	Euler roll angle in relative velocity coordinate frame for lift vector
Delta bu_time2	Time between initial breakup and secondary breakup
Beta1	Ballistic coefficient following first breakup for cases with two breakups
DX Mag	Magnitude of the delta position vector at separation

Table 3: Summary of Trajectory Reconstructions

Method	Configuration	Piece	Impact Error	Bu_time1	DV Mag	L/D	Roll Angle	Delta bu_time2	Beta1	DX Mag
			(feet)	(sec)	(fps)		(deg)	(deg)	(lbs/ft^2)	(feet)
1	random_tumble	1	0	50421.01	379.15					
1	trimmed	1	0	50424.44	164.65					
1	random_tumble	2	0	50435.47	328.90					
2	random_tumble	2	0	50435.45		0.0289	102.20			
3	random_tumble	2	-0.87	50470.27				109.32	7.70	
4	random_tumble	2	0	50439.9	172.07					5396.78
1	random_tumble	3	0	50435.58	458.63					
2	random_tumble	3	0	50435.66		0.0318	-270.97			
3	random_tumble	3	33.92	50462.08				20.80	1.50	
4	random_tumble	3	0	50438.19	188.05					7343.86
1	random_tumble	4	0	50437.69	152.47					
2	random_tumble	4	0	50434.63		0.0917	74.29			
3	random_tumble	4	0	50451.99				53.86	13.70	
4	random_tumble	4	0	50426.03	13.78					497.09
1	random_tumble	5	0	50425.02	113.20					
2	random_tumble	5	0	50436.11		0.0838	196.32			
3	random_tumble	5	-0.31	50424.58				70.94	15.80	
4	random_tumble	5	0	50424.73	33.23					1642.98

A description of the results for each object follows.

4.1 Debris #1

Trajectory reconstructions for Debris #1, the payload bay door fragment, were performed using reconstruction method #1. Separate cases were analyzed assuming trimmed and random tumbling configurations. Assuming a tumbling entry configuration, a delta-V of 379.15 ft/sec with a breakup time of 50421.01 seconds was required to cause the object to impact at the proper location. If a trimmed aerodynamic configuration is assumed, the breakup time moves to 50424.44 sec and the delta-V at breakup decreases to 164.65 ft/sec. Recall that the *Columbia* main body breakup was known to occur at 50421 sec, thus the payload door fragment very likely separated from the Orbiter within 3 seconds after the main body breakup.

4.2 Debris #2

Trajectory reconstructions for Debris #2, the 40-inch diameter COPV weighing 262 lbs, were performed using all four reconstruction methods. For all of the spheres, a random tumbling configuration with a hypersonic continuum drag coefficient of 0.92 was used. However, due to symmetry, tumbling and fixed attitude for a sphere would be indistinguishable from an aerodynamic standpoint. The four reconstruction methods had initial breakup times between 50435.45 and 50470.27 sec. Reconstruction method #1 required a delta-V of 328.9 ft/sec to match the impact location. A relatively small lift-to-drag value of 0.0289 was required with reconstruction method #2. Reconstruction method #3 had the latest initial breakup at 50470.27 sec with initial ballistic coefficient of 7.70 lbs/ft^2. In this case, the secondary breakup that separated this item from some larger piece occurred 109.32 sec after the initial breakup. Reconstruction method #4 required a delta-V of 172.07 ft/sec and a delta-X of 5386.78 feet to match the debris impact location. The position difference of nearly one nautical mile between the base trajectory and the Debris #2 initial displacement from this trajectory is reasonable considering the uncertainty in the breakup dynamics.

An additional trajectory reconstruction modeling a constant direction side (lift) force induced by spinning of Debris #2 was performed. In this case, the model from Ref. [4] that predicts aerodynamic side force for spheres based on spin rate, Reynolds number, radius of the sphere and velocity was incorporated into the TOP simulation. The magnitude of the spin rate and the direction of the side force were each treated as parameters that were varied during the optimization process. The final impact location in the trajectory simulation was constrained to match the known value. The initial breakup time was minimized. The trajectory reconstruction results for this case yielded a breakup time of 50434.29 sec, a spin rate of 18.05 rad/sec and side force direction of 83.86 deg. The breakup time is within 1 sec of the value obtained using reconstruction method #2 for this debris piece. The direction of the side force is approximately 25 deg less than that for reconstruction method #2. The spin rate of 18.05 rad/sec (2.87 revolutions per second) is lower than any of the data points from Ref. [4], while the peak Reynolds numbers for this case (4,420,000) is an order of magnitude larger than the values from Ref. [4]. This calculation indicates that spin-generated lift is a plausible

mechanism for generating the cross-track displacement of the spherical body. But plausibility does not prove that this in fact, what actually happened.

4.3 Debris #3

Trajectory reconstructions for Debris #3, the 18-inch diameter COPV weighing 26 lbs, were performed using all four reconstruction methods. The four reconstruction methods had initial breakup times between 50435.58 and 50462.08 sec. Reconstruction method #1 required a delta-V of 458.639 ft/sec to match the impact location. A relatively small lift-to-drag value of 0.0318 was required with reconstruction method #2. Reconstruction method #3 had the latest initial breakup at 50462.08 sec with initial ballistic coefficient of 1.50 lbs/ft^2. In this case, the secondary breakup that separated this item from some larger piece occurred 20.80 sec after the initial breakup. Finally, with reconstruction method #4, a delta-V of 188.05 ft/sec and a delta-X of 7343.86 feet were required to match the debris impact location. The position difference of over one nautical mile between the base trajectory and the Debris #3 initial displacement from this trajectory is the largest magnitude for any of the debris piece reentry reconstructions.

4.4 Debris #4

Trajectory reconstructions for Debris #4, the 26-inch diameter COPV weighing 72 lbs, were performed using all four reconstruction methods. The four reconstruction methods had initial breakup times between 50426.03.45 and 50451.99 sec. Reconstruction method #1 required a delta-V of 152.47 ft/sec to match the impact location. A larger lift-to-drag value of 0.0917 was required with reconstruction method #2. Reconstruction method #3 had the latest initial breakup at 50451.99 sec with initial ballistic coefficient of 13.30 lbs/ft^2. In this case, the secondary breakup that separated this item from some larger piece occurred 53.86 sec after the initial breakup. Finally, with reconstruction method #4, a delta-V of only 13.78 ft/sec and a delta-X of 497.09 feet were required to match the debris impact location.

4.5 Debris #5

Trajectory reconstructions for Debris #5, the 26-inch diameter COPV weighing 53 lbs, were performed using all four reconstruction methods. The four reconstruction methods had initial breakup times between 50424.58 and 50436.11 sec. Reconstruction method #1 required a delta-V of 113.20 ft/sec to match the impact location. A larger lift-to-drag value of 0.0838 was required with reconstruction method #2. This method also had the latest initial breakup time of 50436.11 sec. Reconstruction method #3 required an initial ballistic coefficient of 15.80 lbs/ft^2 following breakup. In this case, the secondary breakup that separated this item from some larger piece occurred 70.94 sec after the initial breakup. Finally, with reconstruction method #4, a delta-V of 33.23 ft/sec and a delta-X of 1642.98 feet were required to match the debris impact location.

4.6 Data Analysis

Data plots and tables have been generated for the debris trajectory reconstructions. This data was computed along the debris reentry portion of the trajectory following the initial breakup. The heating rate calculation is from Ref. [5]. The following quantities were computed for data analysis

$$\text{Dynamic pressure } q = 0.5\rho v^2 \ \left(\text{lb/ft}^2\right)$$

where ρ = density $\left(\text{slug/ft}^3\right)$

v = air relative velocity (ft/sec)

$$\text{Sensed acceleration} = q\,S\,\sqrt{C_D^2 + C_L^2}\Big/m \ \left(\text{ft/s}^2\right)$$

where S = aerodynamic reference area $\left(\text{ft}^2\right)$

C_D = drag coefficient

C_L = lift coefficient

m = mass (slugs)

$$\text{Heating rate} = \dot{q} = 104\sqrt{\frac{1}{R}}\sqrt{\frac{\rho}{\rho_{SL}}}\left(\frac{v}{10{,}000}\right)^{3.15} \ \left(\text{BTU/ft}^2/\text{sec}\right)$$

where R = body radius (ft)

ρ = density $\left(\text{slug/ft}^3\right)$

ρ_{SL} = density at sea level $\left(\text{slug/ft}^3\right)$

v = air relative velocity (ft/sec)

$$\text{Total Heating} = \int \dot{q}\,dt$$

Data plots for Debris #1 showing the heating rate, sensed acceleration and dynamic pressure assuming random tumbling are shown in Figures 10. Figure 11 shows the velocity and altitude profiles versus time for this same object with random tumbling aerodynamics. In Figure 12, the heating rate, sensed acceleration and dynamic pressure assuming trimmed aerodynamics are shown. Figure 13 shows the velocity and altitude profiles versus time for Debris #1 with trimmed aerodynamics. Table 4 summarizes the peak values for several quantities of interest from the Debris #1 trajectory reconstructions.

Table 4: Summary of Trajectory Reconstructions for Debris # 1

Reconstruction Method	1 – trimmed	1-random tumble
Max Altitude (ft)	176803.4	179425.3
Max Relative Velocity (ft/sec)	15648.79	16165.93
Max Mach Number	14.838	15.383
Max Dynamic Pressure (psf)	167.603	162.387
Max Heating Rate (BTU/ft^2 – s)	7.93558	8.347
Max Sensed Acceleration (g's)	57.79	44.53
Total Heating (BTU/ft^2)	2.95	3.85

Table 5 summarizes the peak values for several quantities of interest from the Debris #2 trajectory reconstructions. Reconstruction methods 1, 2 and 4 show very similar peak values due to the small variation of 4 sec in the initial breakup times. Reconstruction method #3 shows the smallest values for altitude, velocity and total heating since the initial breakup time was approximately 30 sec after the other methods. For reconstruction method #3, the large dynamic pressure and heating values occurred at the initial breakup and then rapidly decrease. Figure 14 illustrates data plots for Debris #2 showing the heating rate, sensed acceleration and dynamic pressure for the fourth reconstruction method. The velocity and altitude profiles versus time for the fourth reconstruction method are shown in Figures 15.

Table 5: Summary of Trajectory Reconstructions for Debris # 2

Reconstruction Method	1	2	3	4
Max Altitude (ft)	165885.2	165907.2	119295	158876.9
Max Relative Velocity (ft/sec)	15147.63	15157.24	12459.17	14997.56
Max Mach Number	14.24381	14.25226	12.2587	14.02413
Max Dynamic Pressure (psf)	261.9	259.2182	1064.551	305.4741
Max Heating Rate (BTU/ft^2 – s)	8.44765	8.460303	12.19796	9.322976
Max Sensed Acceleration (g's)	7.288896	7.217211	138.4226	8.501565
Total Heating (BTU/ft^2)	16.29198	16.37328	2.883561	14.74557

Table 6 summarizes the peak values for several quantities of interest from the Debris #3 trajectory reconstructions. Reconstruction methods 1,2 and 4 show very similar peak values due to the small variation of 3 sec in the initial breakup times. Reconstruction method #3 has the smallest values for altitude, velocity and total heating since the initial breakup time was approximately 25 sec after the other methods. For reconstruction method #3, the large dynamic pressure and heating values occurred at the initial breakup and then rapidly decrease. Figure 16 illustrates data plots for Debris #3 showing the heating rate, sensed acceleration and dynamic pressure for the fourth reconstruction method. The velocity and altitude profiles versus time for the fourth reconstruction method are shown in Figures 17.

Table 6: Summary of Trajectory Reconstructions for Debris # 3

Reconstruction Method	1	2	3	4
Max Altitude (ft)	165761.9	165673.6	131538	159812.1
Max Relative Velocity (ft/sec)	15145.63	15150.39	13547.89	15033.75
Max Mach Number	14.24054	14.2425	12.87269	14.06619
Max Dynamic Pressure (psf)	235.7872	236.6516	710.9246	288.62
Max Heating Rate (BTU/ft^2 – s)	12.29775	12.32925	11.77222	13.41123
Max Sensed Acceleration (g's)	15.07854	15.14136	494.066	18.45644
Total Heating (BTU/ft^2)	12.52039	12.51459	2.48656	11.4073

Table 7 summarizes the peak values for several quantities of interest from the Debris #4 trajectory reconstructions. Reconstruction methods 1 and 2 show very similar peak values due to the small variation of 3 sec in the initial breakup times. Reconstruction method #3 has the smallest values for altitude, velocity and total heating since the initial breakup time was approximately 15 sec after the other methods. For reconstruction method #3, the large dynamic pressure and heating values occurred at the initial breakup and then rapidly decrease. In this case, reconstruction method #4 had the earliest breakup time at 50436 sec GMT. This earlier breakup time resulted in higher initial velocity and total heating values compared to the other methods. Figure 18 illustrates data plots for Debris #4 showing the heating rate, sensed acceleration and dynamic pressure for the fourth reconstruction method. The velocity and altitude profiles versus time for the fourth reconstruction method are shown in Figures 19.

Table 7: Summary of Trajectory Reconstructions for Debris # 4

Reconstruction Method	1	2	3	4
Max Altitude (ft)	163427.9	166784.3	145752.7	175378.5
Max Relative Velocity (ft/sec)	15078.37	15182.55	14403.65	15387.5
Max Mach Number	14.14468	14.28842	13.48717	14.57293
Max Dynamic Pressure (psf)	254.2515	228.3885	451.6201	185.05
Max Heating Rate (BTU/ft^2 – s)	10.96467	10.53264	13.34224	9.368048
Max Sensed Acceleration (g's)	10.36897	9.353484	32.29392	7.546609
Total Heating (BTU/ft^2)	14.79339	15.915	7.091293	17.44553

Table 8 summarizes the peak values for several quantities of interest from the Debris #5 trajectory reconstructions. Reconstruction methods 1, 3 and 4 show very similar peak values due to the small variation of 1 sec in the initial breakup times. Reconstruction method #2 shows the smallest values for altitude, velocity and total heating since the initial breakup time was approximately 10 sec after the other methods. Figure 20 illustrates data plots for Debris #5 showing the heating rate, sensed acceleration and dynamic pressure for the fourth reconstruction method. The velocity and altitude profiles versus time for the fourth reconstruction method are shown in Figures 21.

Table 8: Summary of Trajectory Reconstructions for Debris # 5

Reconstruction Method	1	2	3	4
Max Altitude (ft)	176299.1	165180.7	176679.1	174953.4
Max Relative Velocity (ft/sec)	15552.68	15135.9	15634.4	15607.97
Max Mach Number	14.73858	14.22	14.82	14.77471
Max Dynamic Pressure (psf)	168.6599	240.42	168.06	178.25
Max Heating Rate (BTU/ft^2 – s)	9.515693	10.74	9.60	9.85
Max Sensed Acceleration (g's)	9.324166	13.34	10.69	9.85
Total Heating (BTU/ft^2)	14.6135	11.72133	13.85237	14.7202

5. SIMPLIFIED COMPOSITE HEATING MODEL

A simplified composite material ablation model developed for the payload bay door rib structure is described in this section. This model is based on the work in Refs 6 and 8. The four equations displayed in Ref. 6 are:

$$\dot{w} = \rho_s B \exp\left(-E / RT\right) \tag{1}$$

$$\dot{m} = \left\{ \frac{\rho_s k_w(T_w) B T_w}{h_{py}(T_w) - h_b} \right\}^{1/2} \left\{ \frac{R T_w}{E} \right\}^{1/2} \exp\left\{-E/(2RT_w)\right\} \tag{2}$$

$$\dot{q}_{cw} \left\{ 1 - \frac{h_{air}(T_{w)}}{H^0} \right\} - \dot{m} \left\{ h_{py}(T_w) - h_b \right\} = 0 \tag{3}$$

and rearranging (3)

$$\dot{m} = \frac{1 - \dfrac{h_{air}(T_w)}{H^0}}{h_{py}(T_w) - h_b} \, \dot{q}_{cw} \tag{4}$$

In the above equations, $\dot{m}$ denotes the mass flux (kg/sec/m^2) from the surface, i.e., the <u>ablation rate</u>. Additional nomenclature used in the equations is given below.

T_w	=	wall temperature of the ablating surface (K)
ρ_s	=	density of epoxy resin (kg/m^3)
k_w	=	thermal conductivity of pyrolysis gas at wall (W/m/K)
h_{py}	=	enthalpy of pyrolysis gas at wall (J/kg)
h_b	=	base (cold) enthalpy of the epoxy resin (J/kg)
B	=	frequency factor (sec^{-1})
E	=	activation energy (J/mole)
R	=	gas constant (J/mole/K)
h_{air}	=	enthalpy of air (J/kg)
H^0	=	stagnation enthalpy of the external flow (J/kg)

Equations (2) and (4) are two equations for two unknowns: $\dot{m}$ and T_w. Eliminating the mass flux between (2) and (4) gives the following single equation for T_w.

$$\left\{k_w(x)\left[h_{py}(x)-h_b\right]\right\}^{1/2} c_3\, x\, e^{-1/(2x)} \; -\left[1-\frac{h_{air}(x)}{H^0}\right]=0 \tag{5}$$

In (5), the unknown variable, T_w, has been replaced by the dimensionless variable *x*, which is defined as

$$x \equiv T_w / T_E \qquad \text{where} \quad T_E = E/R \tag{6}$$

Also, for brevity, we have let

$$c_3 = \frac{\sqrt{\rho_s B T_E}}{\dot{q}_{cw}} \tag{7}$$

For convenience in coding and discussion, (5) is rewritten as follows

$$f_2(x) = p_2(x) g_2(x) - r_2(x) = 0 \tag{8}$$

where

$$p_2(x) = \left\{k_w(x)\left[h_{py}(x)-h_b\right]\right\}^{1/2} \tag{9}$$

and

$$g_2(x) = c_3\, x\, e^{-1/(2x)} \tag{10}$$

and

$$r_2(x) = 1 - h_{air}(x)/H^0 \tag{11}$$

It is now possible to iteratively solve for the root, *x*, in (8) which drives the residual, f_2, to zero. For example, if x_0 represents an initial estimate of the root, then an improved estimate for *x* may be found by Newton's method.

$$x = x_0 - f_2(x_0)/\, f_2'(x_0) \tag{12}$$

Physical reality dictates the following constraints.

$$x > 0, \quad p_2 > 0, \quad \text{and} \quad 0 \le r_2 < 1 \tag{13}$$

Additionally, the following behavior of g_2 for positive argument is noted.

$$g_2 \to 0 \text{ as } x \to 0 \quad \text{and} \quad g_2 \sim c_3 x \text{ as } x \to \infty \tag{14}$$

Once x is found, the wall temperature and mass flux are calculated as follows.

$$T_w = T_E x \tag{15}$$

$$\dot{m} = \dot{q}_{cw} r_2(x) / \left[h_{py}(x) - h_b \right] \tag{16}$$

Integration of $\dot{m}$ with time over the trajectory gives the total mass loss, Δm, per unit surface area (kg/m^2).

$$\Delta m = \int_0^t \dot{m} dt \tag{17}$$

<u>Cold-wall heat flux</u>

The cold-wall heat flux (averaged over the surface of interest) is approximated by a fraction of the instantaneous cold-wall flux at the stagnation point. Namely,

$$\dot{q}_{cw} = k_2 \; \dot{q}_{s,cw} \tag{18}$$

where k_2 is an area-averaging factor ($0 < k_2 < 1$.) Typically, k_2 is set to a value of 0.12 when modeling the average surface heating to a tumbling reentry body. The cold-wall heat flux at the stagnation point is computed via the Detra, Kemp, Riddell (DKR) correlation.

$$\dot{q}_{s,cw} = 4.47 \text{ x } 10^{-9} \sqrt{\frac{\rho_\infty}{R_{nose}}} \, V_\infty^{3.15} \quad \text{BTU/sec/ft}^2 \tag{19}$$

In the above equation, the density, ρ_∞, nose radius, R_{nose}, and air-relative velocity, V_∞, are entered in English units. The flux in metric units is then obtained with the following conversion.

$$1 \text{ BTU/sec/ft}^2 = 11356.526682227 \text{ W/m}^2 \tag{20}$$

Thus, the cold-wall heat flux depends on the instantaneous values of two trajectory quantities: free stream-density, ρ_∞, and free-stream velocity, V_∞.

Enthalpy of air

The enthalpy of air at commonly-encountered densities is primarily a function of temperature. Tabular data from Ref. 7 was fit with a quadratic equation. The results are plotted in Figure 22. With enthalpy in kJ/kg and temperature in Kelvin, the equation which fits the data is

$$h_{air} = 169.69453 + 0.93675755\ T + 9.8415224 \text{ x } 10^{-5}\ T^2 \tag{21}$$

Stagnation enthalpy of the external flow

This is taken to be the stagnation enthalpy of the free stream, which is computed as follows

$$H^0 = h_{air}(T_\infty) + V_\infty^2 / 2 \tag{22}$$

where T_∞ is the free stream static temperature, and V_∞ is the free-stream velocity.

Model Constants

The following values of model constants are recommended (Ref. 6) for the graphite-epoxy material used in the construction of the Space Shuttle *Columbia*'s Payload Bay door.

$$T_E = 18,707.5 \text{ K} \tag{23}$$

$$B = 3.4 \text{ x } 10^9 \text{ sec}^{-1} \tag{24}$$

$$\rho_s = 1268.66 \text{ kg/m}^3 \tag{25}$$

$$h_b = -9.95528 \text{ x } 10^5 \text{ J/kg} \tag{26}$$

Model Temperature Functions

The following functions are recommended (Ref. 6) for the graphite-epoxy material used in the construction of the Space Shuttle *Columbia*'s Payload Bay door.

$$h_{py} = 2512.08\left(T_w - 300\right) + 3349.44\left(T_w - 500\right) \text{ J/kg} \tag{27}$$

$$k_w = 2.118419 \text{ W/m/K} \tag{28}$$

6. ABLATION MODEL PREDICTIONS FOR PAYLOAD BAY DOOR RIB STRUCTURE

The above model is now applied to the payload bay door reentry. As Figures 23 and 24 show, the exterior surface of the payload bay door shows severe charring in areas where the insulation was removed. The interior surface shows no apparent damage except near the exposed rib structure. These observations support the conclusion that the exterior surface was facing the air stream during portions of the reentry where heating was significant.

The ablation model was coded and interfaced with the TOP reentry trajectory simulation. The reentry trajectory simulation for the payload bay door assuming a trimmed attitude was repeated using the reconstructed debris separation time of 50424.44 sec. For computing the stagnation heat flux on the exposed rib area, the nose radius was assigned the following value.

$$R_{nose} = 0.0546875 \text{ ft} \tag{29}$$

Cases were run with the following values of the area-averaging parameter

$$k_2 = 0.12,\ 0.8,\ \text{and}\ 1.0 \tag{30}$$

The results are summarized in Figures 25, 26 and 27. In Figure 25, the predicted wall temperature is plotted versus altitude over a 20 second period for three values of k_2. The peak temperature values, ranging from 550 to 720 deg C, all occur at breakup and rapidly decrease with time. In Figure 26, the cumulative predicted mass loss is plotted versus time from breakup. For the three values of k_2, most of the mass loss occurs in the first 10 seconds after breakup. The total predicted mass loss as a function of the heating parameter k_2 is shown in Figure 27. This figure shows that the total mass loss is closely approximated as a linear function of the heating parameter k_2.

Laboratory analyses of payload bay door graphite epoxy samples were performed by Dr. Gary Steckel of the Materials Science Department at The Aerospace Corporation. Four samples from the payload bay door ribs, and a single sample from the payload bay panel area were analyzed. These analyses included optical microscopy to assess physical damage, Dynamic Mechanical Analysis (DMA) to measure epoxy glass transition temperature, and Thermal Gravimetric Analysis (TGA) to determine decomposition characteristics. Significant findings from this analysis include

1. Payload bay door debris piece initially reentered with exterior surface exposed to the air stream.
2. Little or no damage to interior of payload bay door.
3. Exposed areas of payload bay door ribs (area 3 and 4) saw significant charring and mass loss during reentry
4. Estimated peak temperature for rib area #4 was between 500 and 650 deg C
5. Estimated mass loss for rib area #3 was 0.23 gm/cm^2
6. Estimated mass loss for rib area #4 was 0.24 gm/cm^2

In Figure 27, the value of $k_2 = 0.8$ which yields a predicted mass loss of 0.24 gm/cm^2 that agrees with the laboratory analysis is noted. This is the suggested calibrated value for the heat flux parameter k_2 for the new composite material ablation model.

7. CONCLUSIONS

This report describes trajectory reconstruction and heating analysis for several composite debris items recovered following the tragic loss of the *Columbia* space shuttle. The goal of this work is to further our understanding of reentry breakup dynamics and space vehicle component survivability. NASA's efforts to recover and catalogue *Columbia* debris, and loan debris to researchers provides a unique opportunity for advancing reentry breakup modeling techniques. Composite debris items recovered from *Columbia* were the focus of this study since prior to this accident, there were no documented cases where composite material items not designed to ablate had been recovered from a reentering stage or spacecraft.

Eight composite *Columbia* debris items were delivered to The Aerospace Corporation for this study. These eight pieces consisted of three odd-shaped fragments, four gaseous tanks, and a single irregularly shaped portion of the payload bay door. Because the three odd-shaped skin fragments were very light and showed little evidence of reentry heating, they were not analyzed. The five remaining objects all showed degradation due to reentry heating. The aerodynamic characteristics for each object were estimated based on their weight and dimensions. For the four spheres, the hypersonic continuum drag coefficients were estimated including transonic and subsonic drag changes. For the payload bay door fragment, the drag coefficient was estimated for both trimmed and tumbling attitudes. Reentry trajectory profiles for each debris piece were then estimated using trajectory simulation and optimization techniques. An Aerospace Corporation reentry trajectory profile for the intact orbiter (pre-break-up), and lead object (post-breakup), was developed shortly after the *Columbia* accident. Each debris object was assumed to emanate from this trajectory profile with the breakup time varied from case to case. Because of the uncertainty in modeling the breakup dynamics, four different methods were considered. These methods were: single breakup with an instantaneous velocity change (delta-v) at breakup; single breakup with lift force; double breakup with larger intermediate debris object; and single breakup with instantaneous velocity (delta-v) and position (delta-x) changes at breakup. Optimization techniques were then used to vary the independent variables (breakup time, delta-v, delta-x, lift, etc.) so that the impact location of the debris piece landed exactly, or close to, the observed impact location. From these trajectory reconstructions, estimates for heating rate, total heating, and aerodynamic loads experienced by each recovered item were determined.

The results from this trajectory reconstruction analysis for the four spheres showed that with a single breakup (first, second and fourth methods), initial breakup times and subsequent reentry trajectory profiles were very similar in each case. The third method with a double breakup yielded larger variations. Through analysis of the ablation and estimated heating experienced by each debris object, it might be possible to discard some breakup scenarios, or strengthen the case for others. By analyzing impact locations of duplicates of the four

spheres, or debris that impacted near each of the spheres, additional insight into each sphere's reentry dynamics might be gained. These additional analyses were beyond the scope of the current study, but should be considered as potential follow-on work

A more detailed heating and ablation analysis was completed for the payload bay door debris piece. Through Aerospace Corporation internal funding, laboratory analysis of the payload bay door composite rib structure was completed, and a simplified composite material ablation model was developed. The laboratory analysis concluded that during early portions of its reentry, the payload bay door debris piece was in a trimmed attitude with the outside of the door facing the air stream. The amount of material lost due to reentry heating was measured as 0.24 gm/cm^2 for two areas of the exposed rib structure. Based on the reconstructed trajectory profile assuming a trimmed attitude, the new composite material ablation model was used to predict the mass loss on the rib structure for a range of area averaging heating factors (k_2). It was determined that a value of $k_2 = 0.8$ yielded a predicted mass loss that agreed with the observed value.

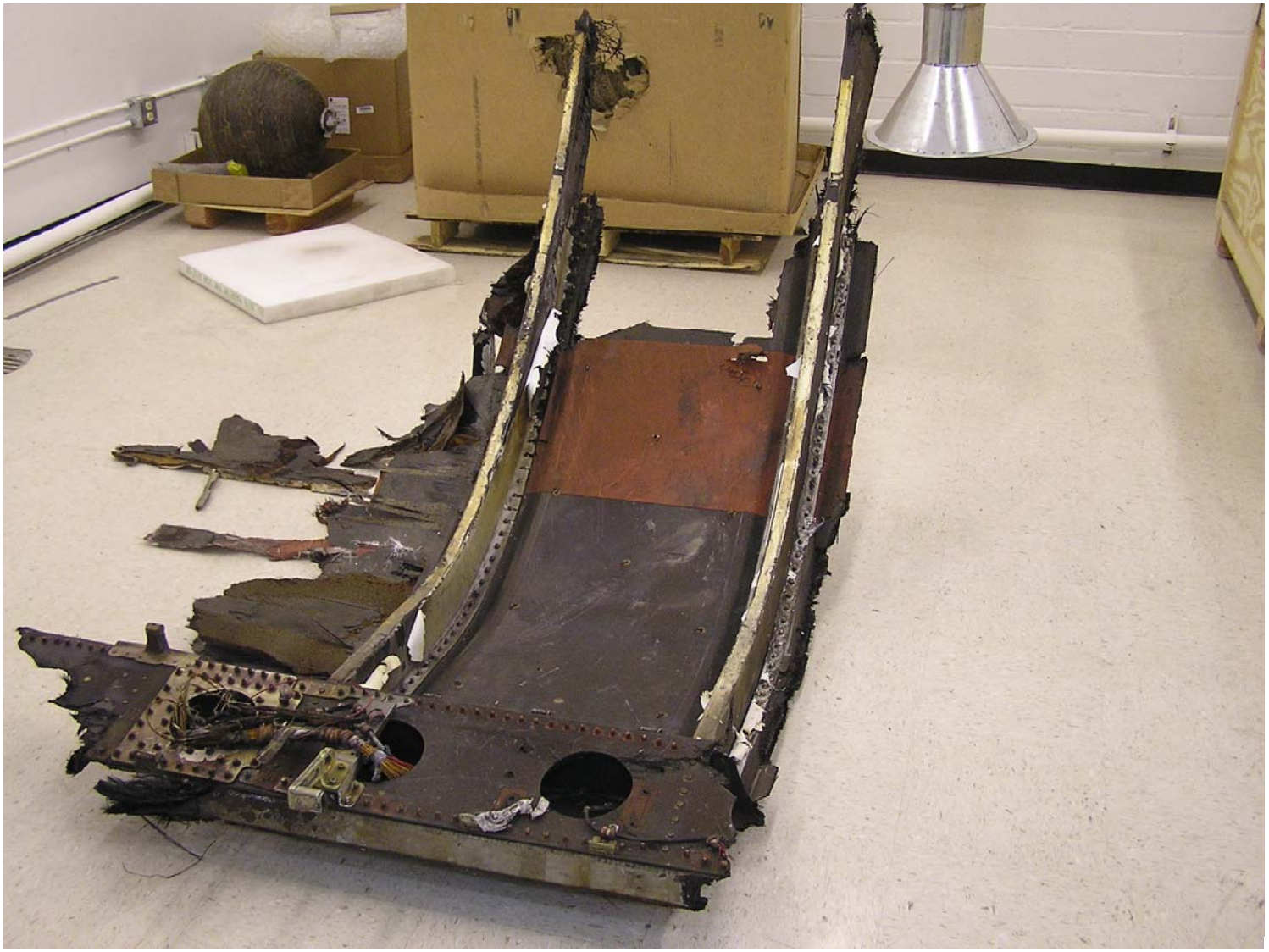

Figure 1: Payload Bay Door # 53993

Figure 2: MPS/OMS Kevlar Helium Tank # 1119

Figure 3: RCS Helium Tank # 38913

Figure 4: Kevlar Wound Tank #49386

Figure 5: Kevlar Wound Tank # 147

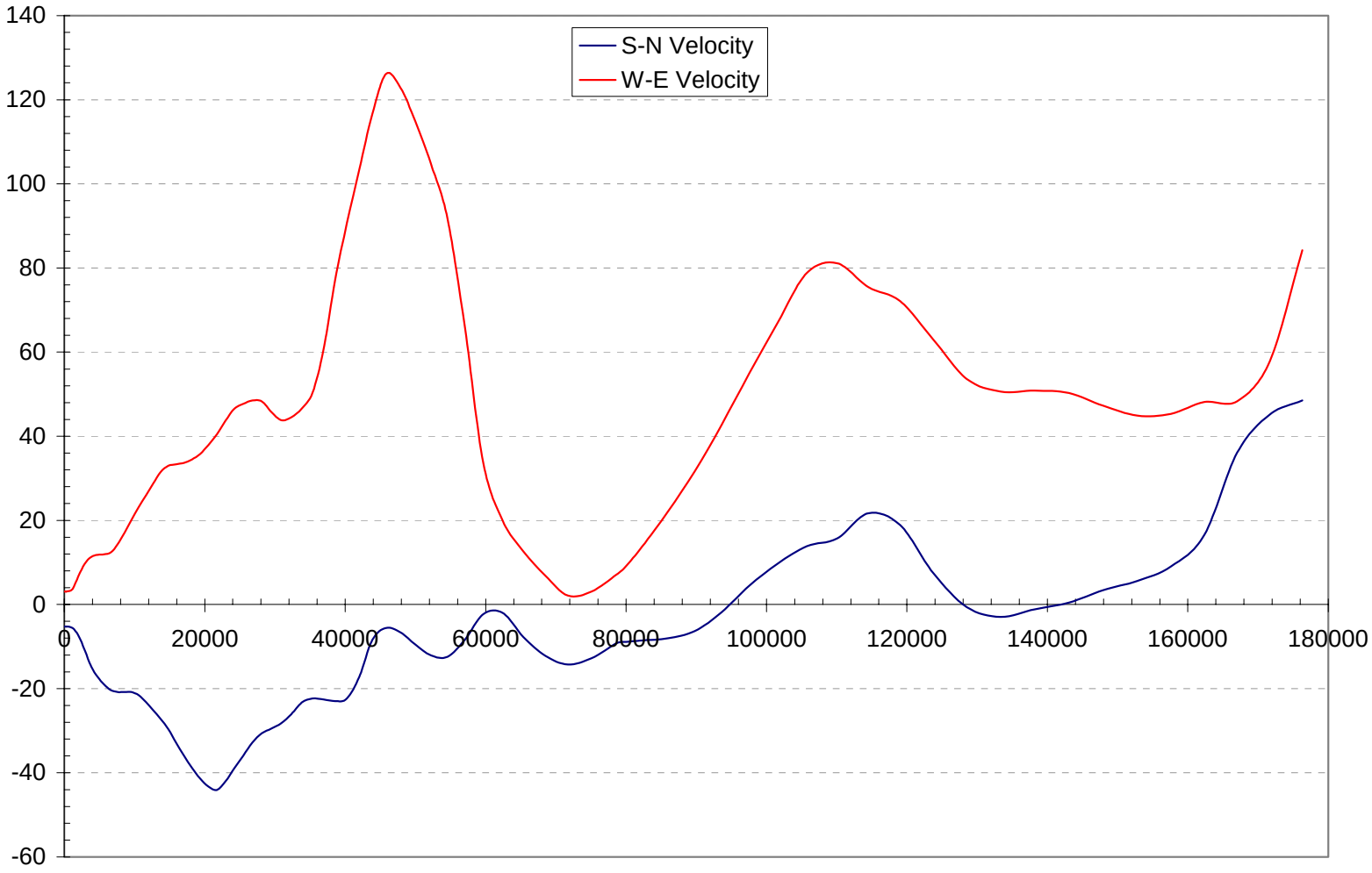

Figure 6: Wind Profile Along Debris #5 Reentry Trajectory

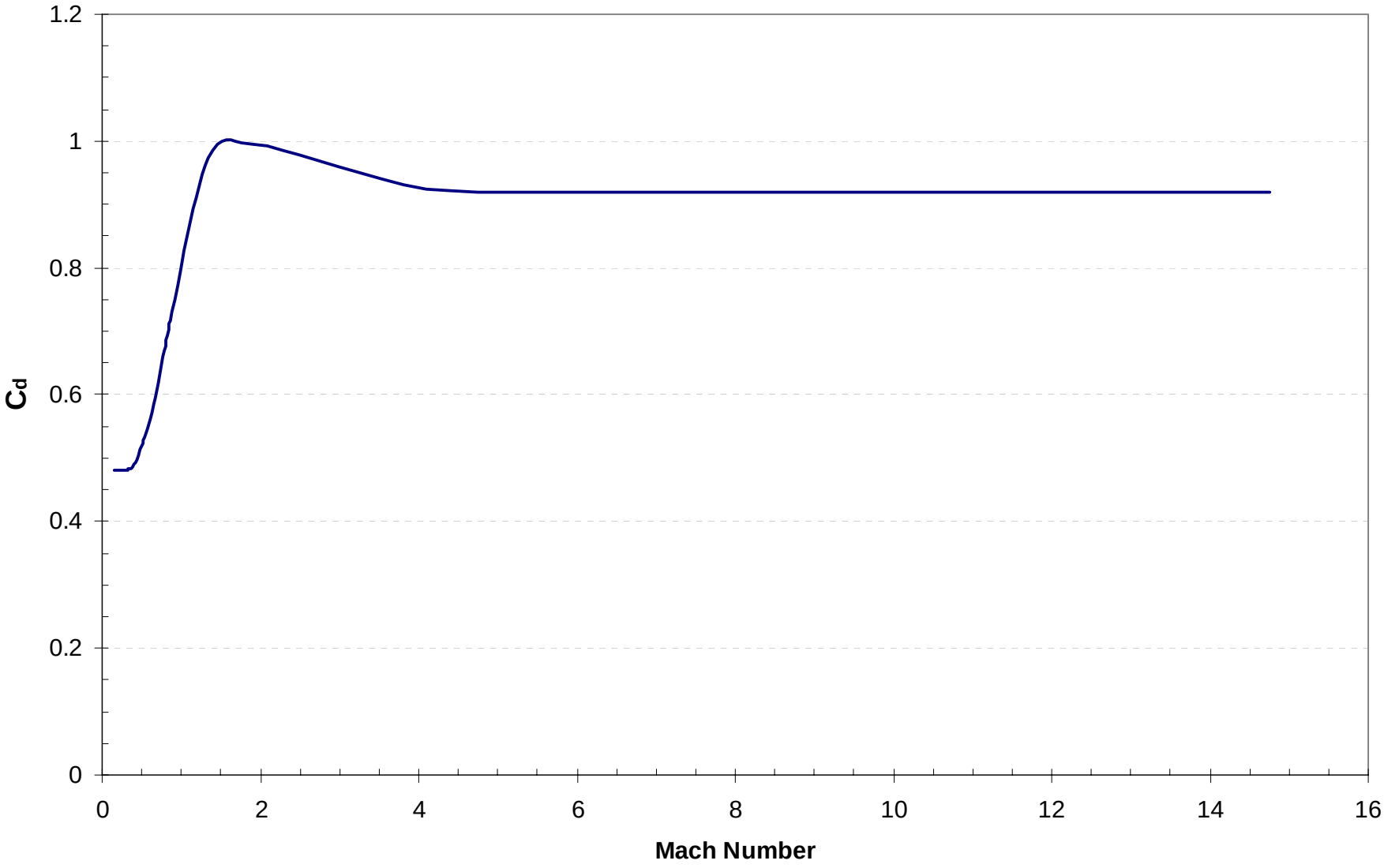

Figure 7: C_d vs Mach Number for Debris #5

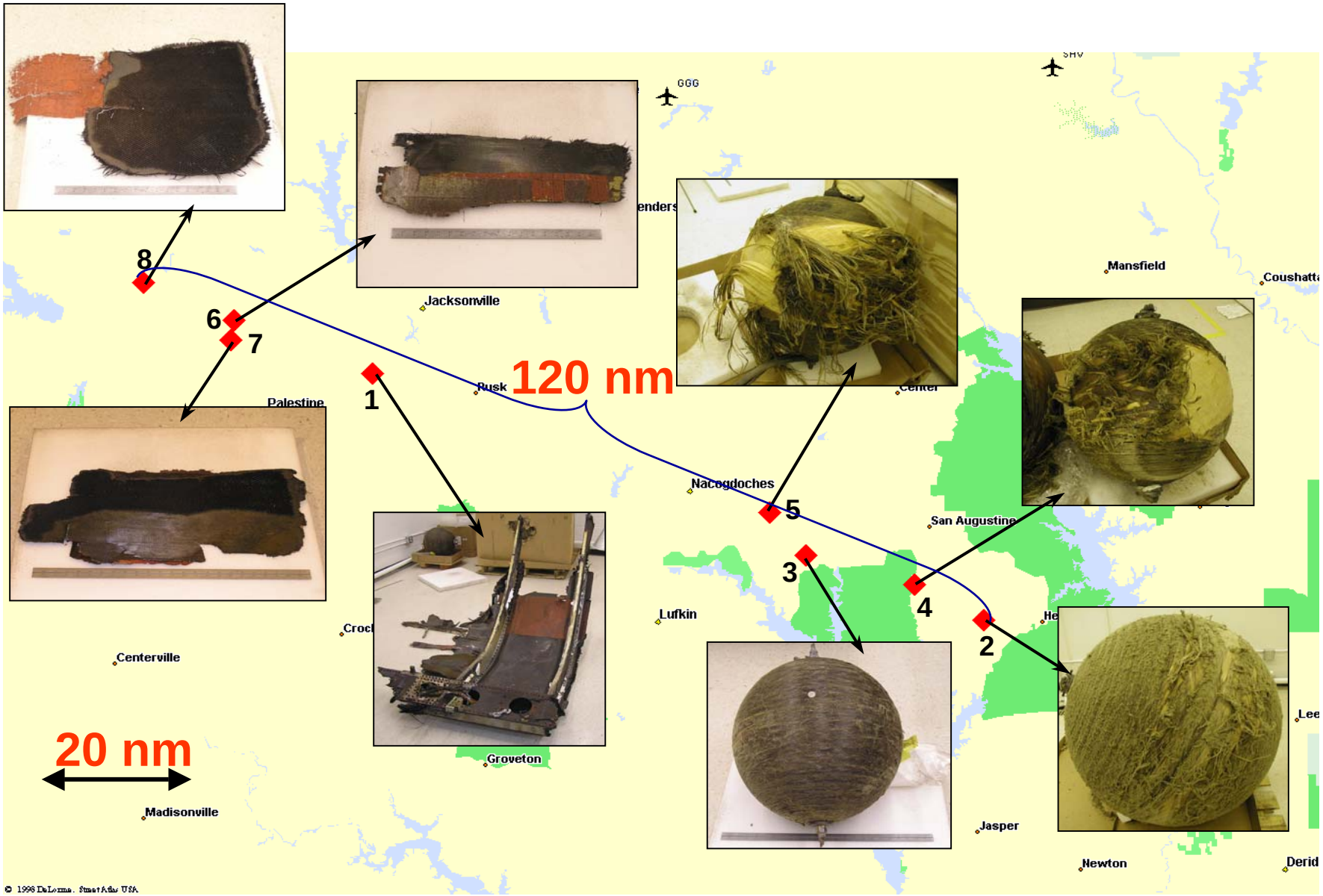

Figure 8: Impact Locations and Debris Pictures

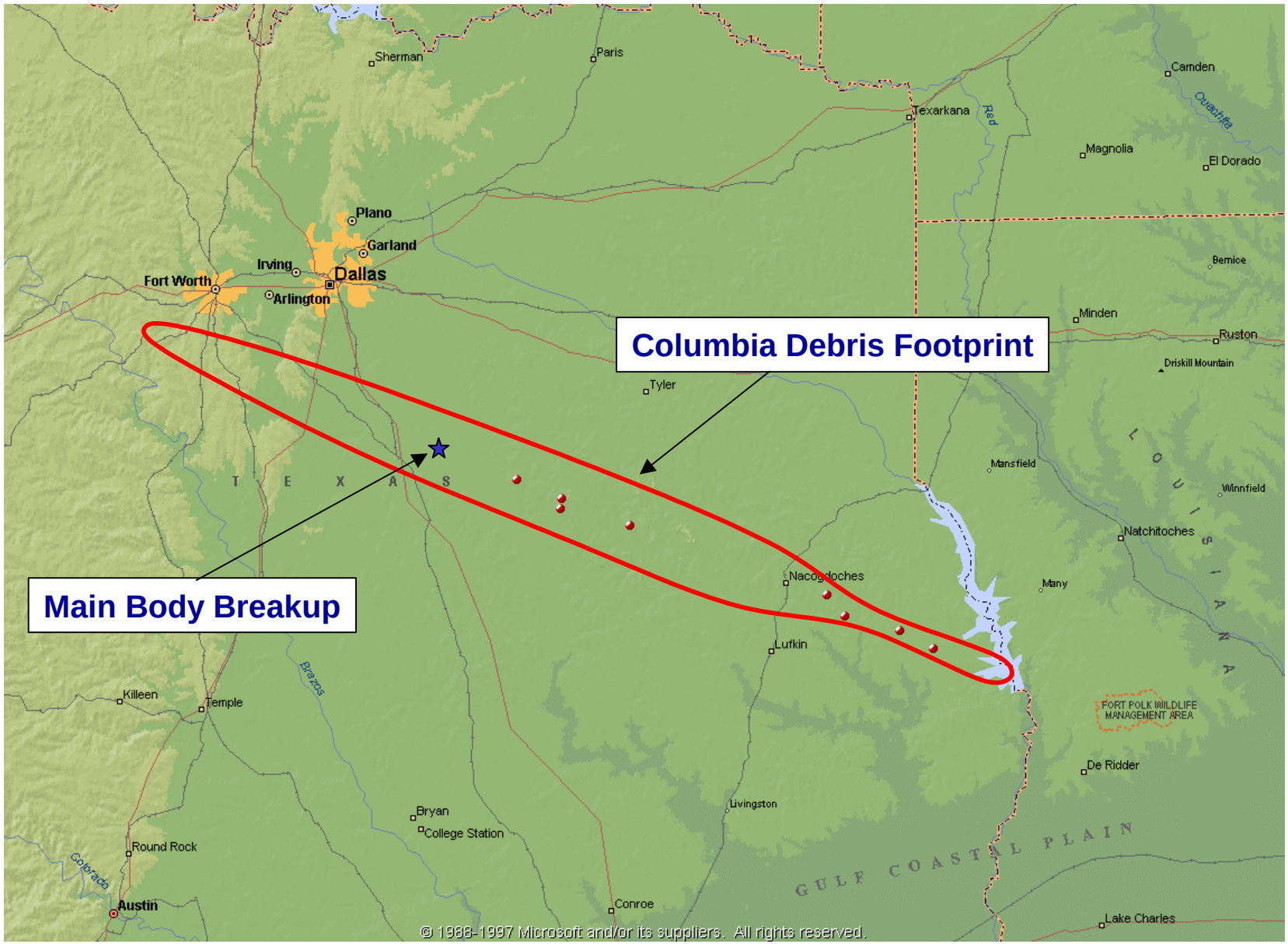

Figure 9: *Columbia* Debris Footprint and Composite Debris Impact Locations

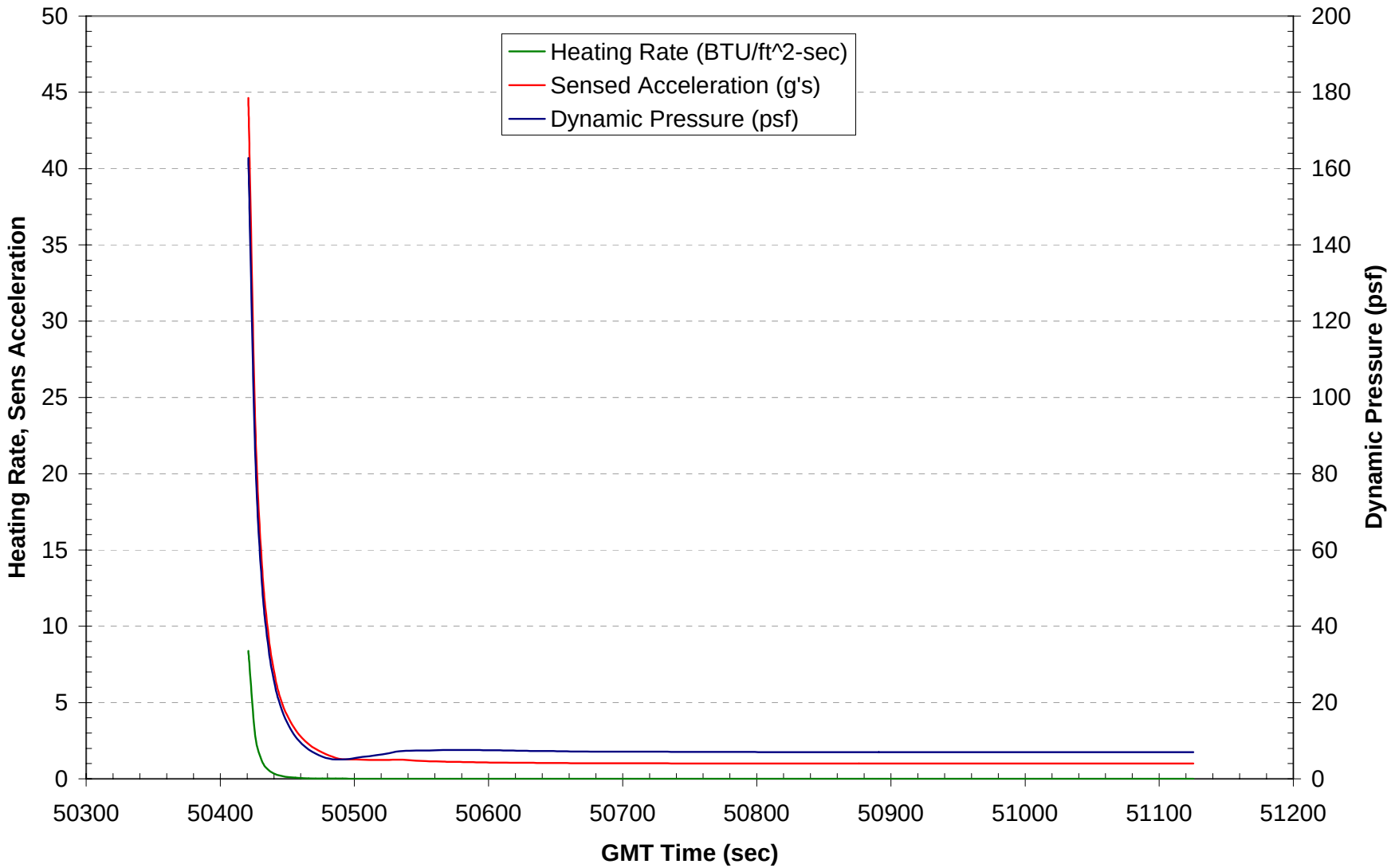

Figure 10: Reentry Heating and Loads Data for Debris #1 Random Tumbling Aerodynamics - Method 1

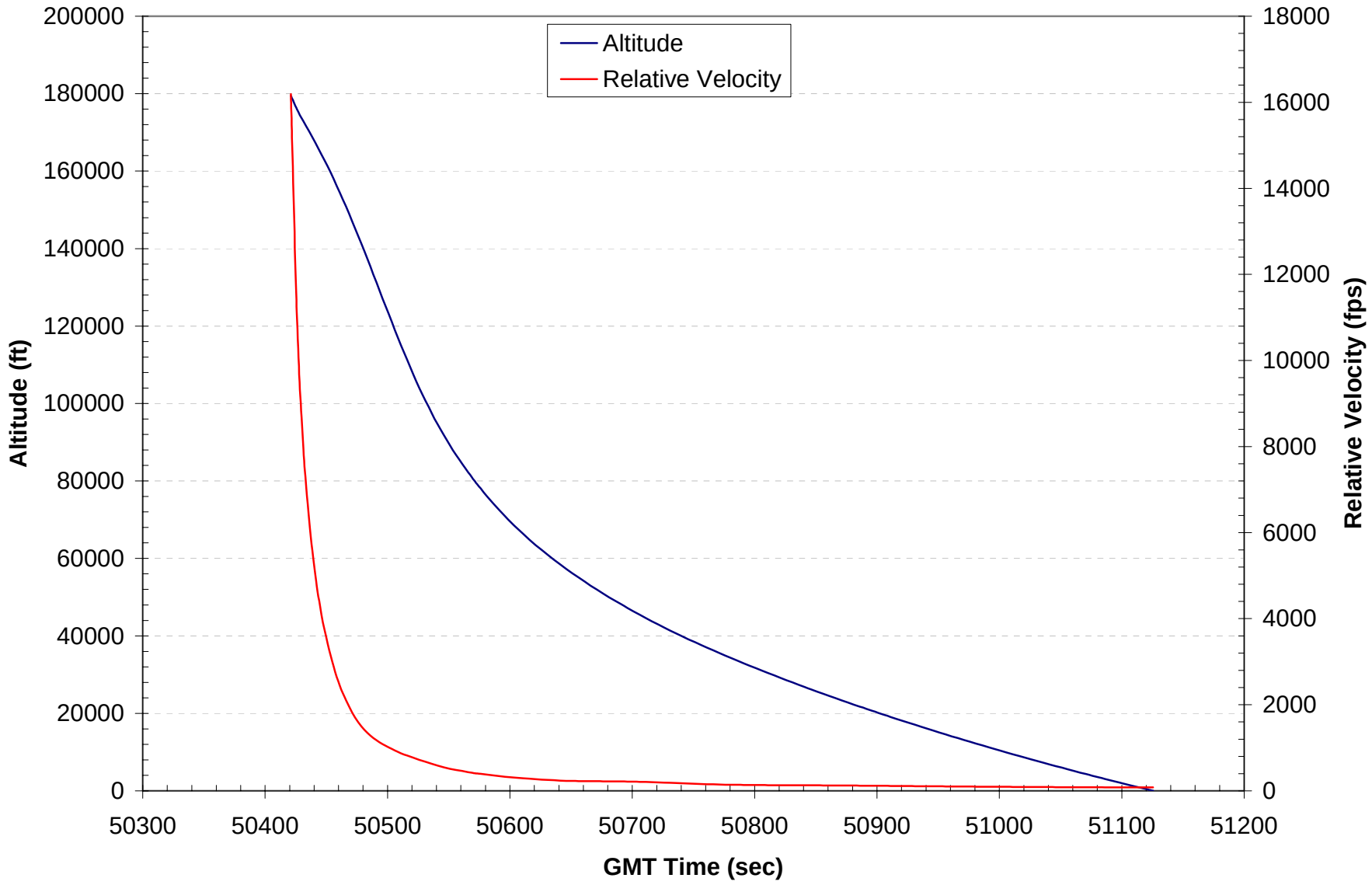

Figure 11: Reentry Altitude and Velocity Data for Debris #1 Random Tumbling Aerodynamics - Method 1

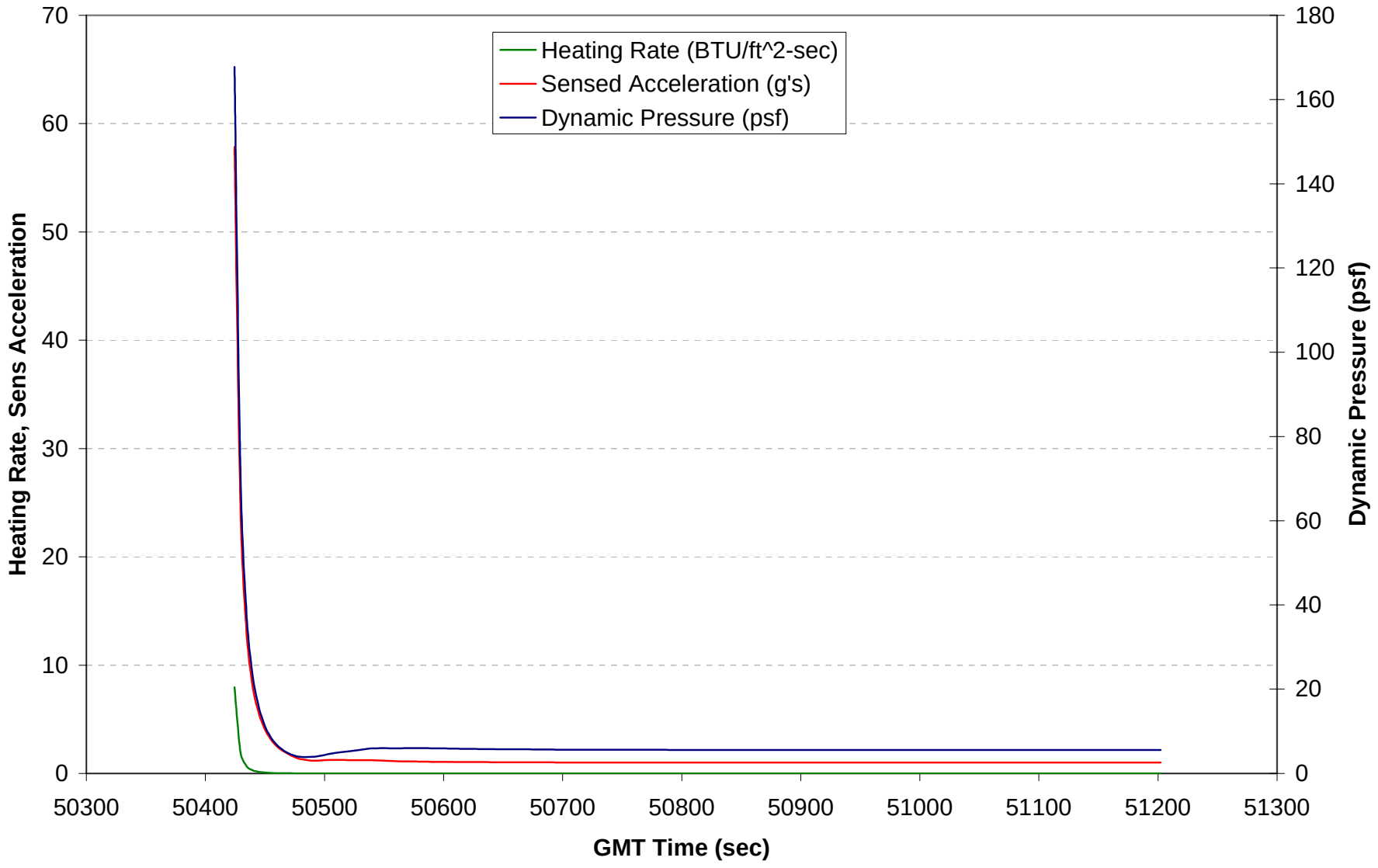

Figure 12: Reentry Heating and Loads Data for Debris #1 Trimmed Aerodynamics - Method 1

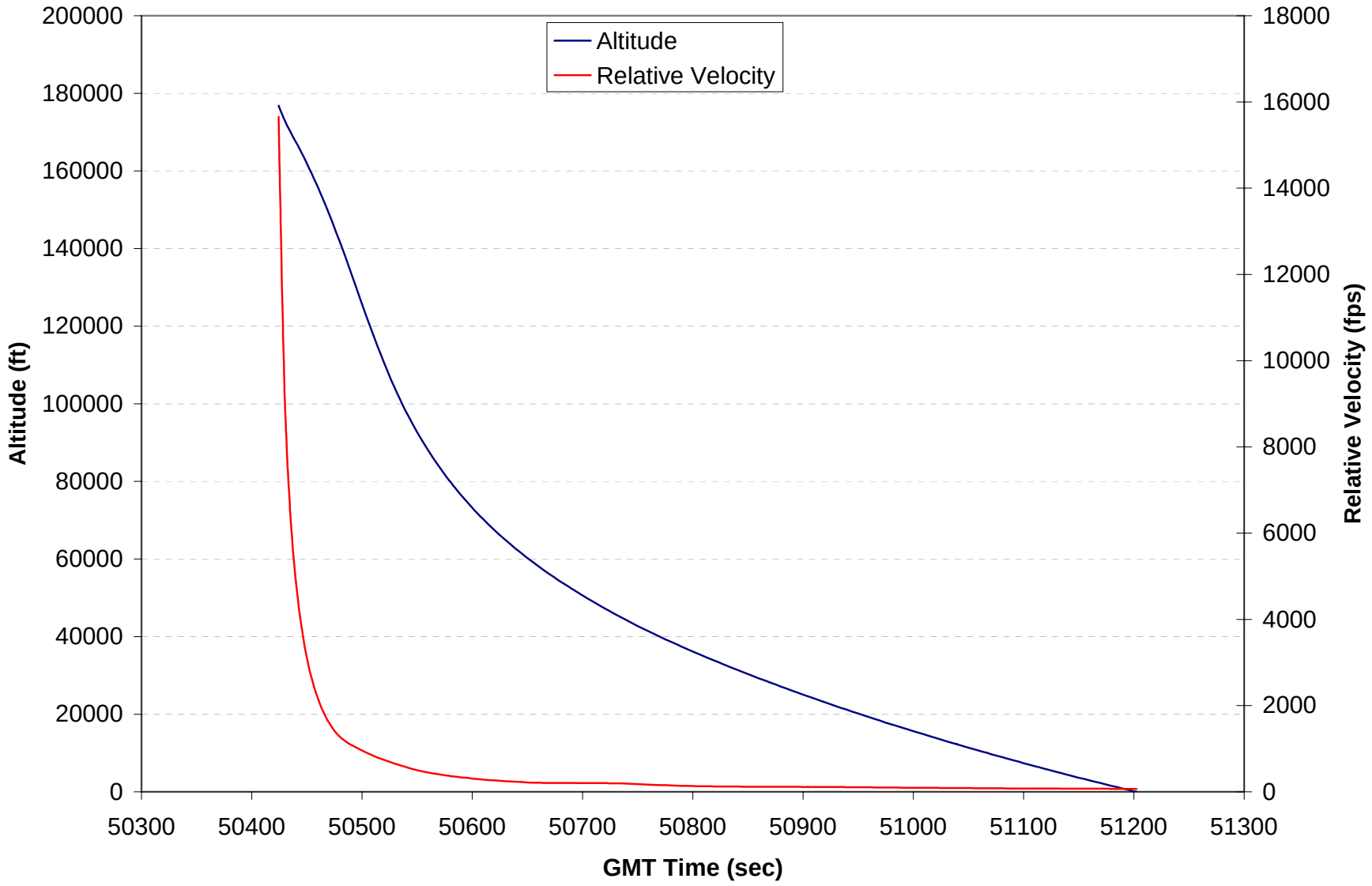

Figure 13: Reentry Altitude and Velocity Data for Debris #1 Trimmed Aerodynamics - Method 1

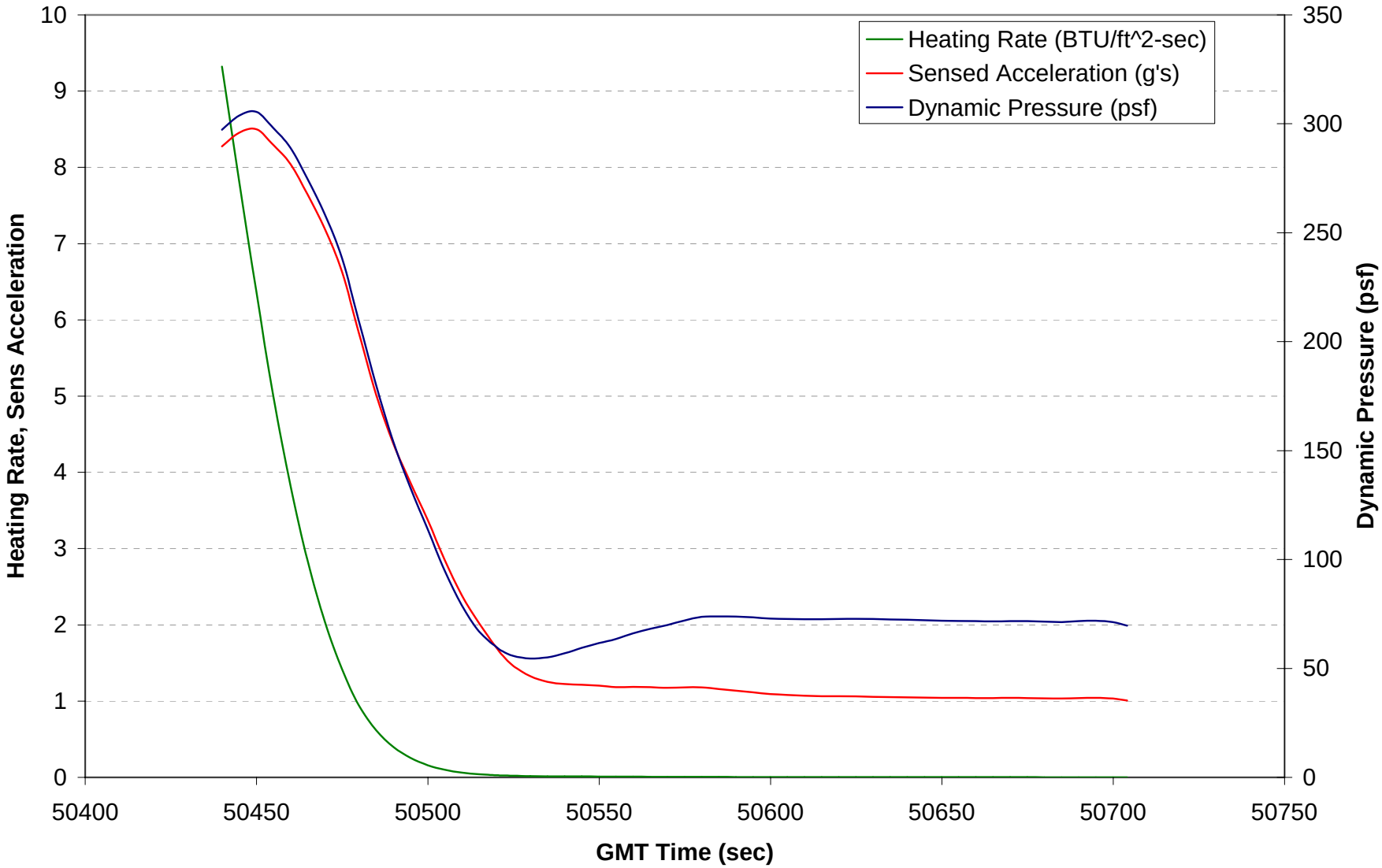

Figure 14: Reentry Heating and Loads Data for Debris #2 Method 4

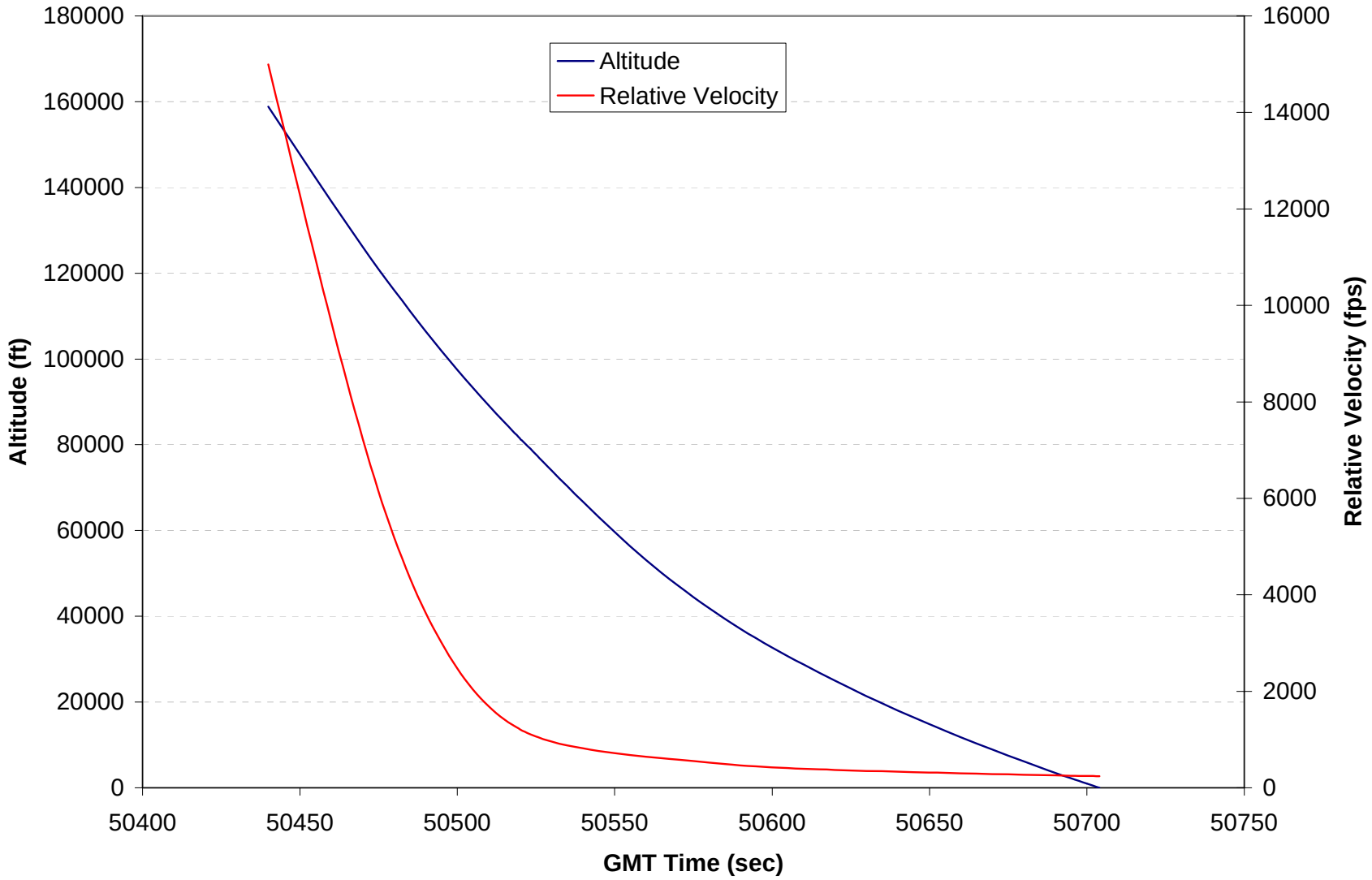

Figure 15: Reentry Altitude and Velocity Data for Debris #2 Method 4

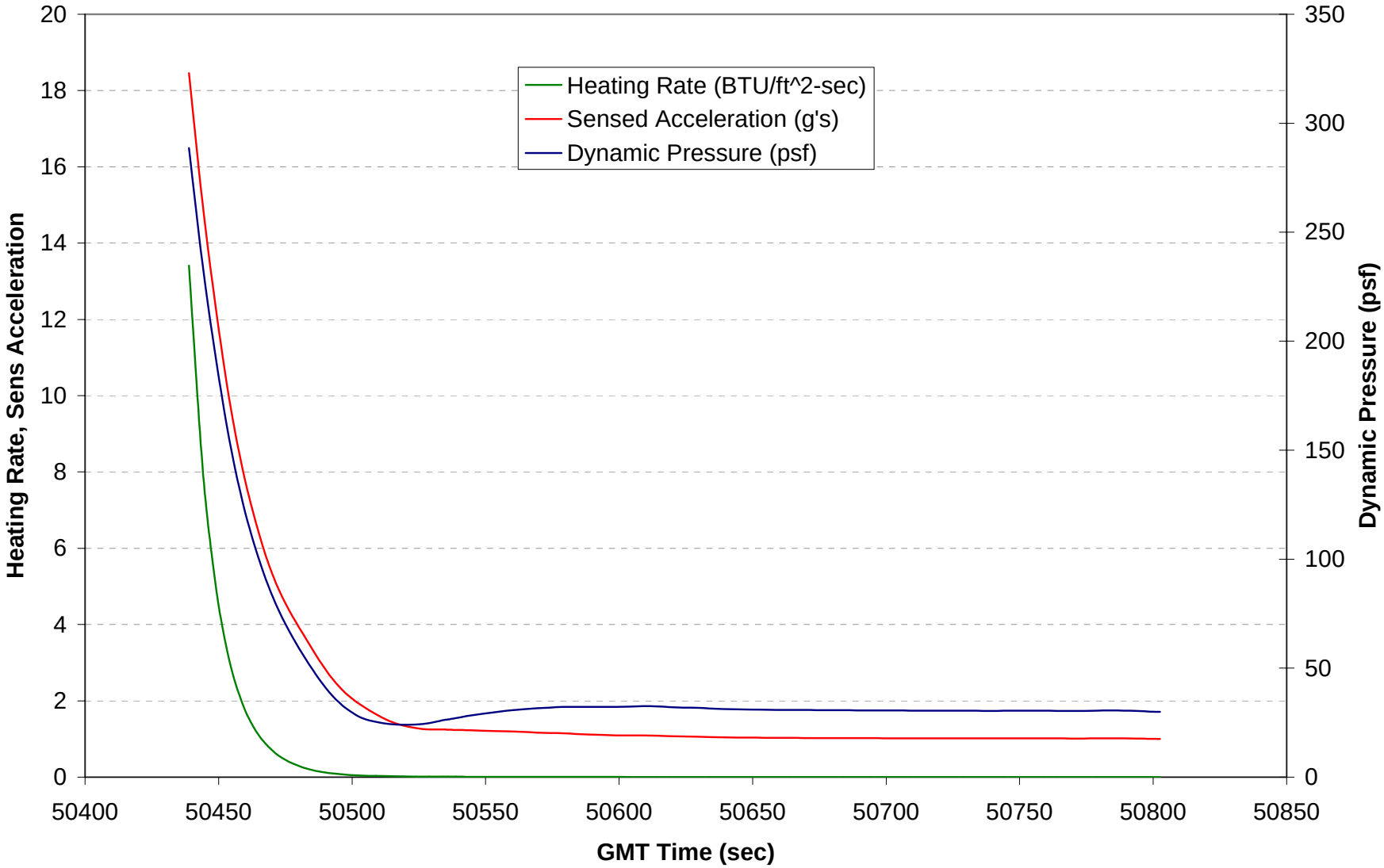

Figure 16: Reentry Heating and Loads Data for Debris #3 Method 4

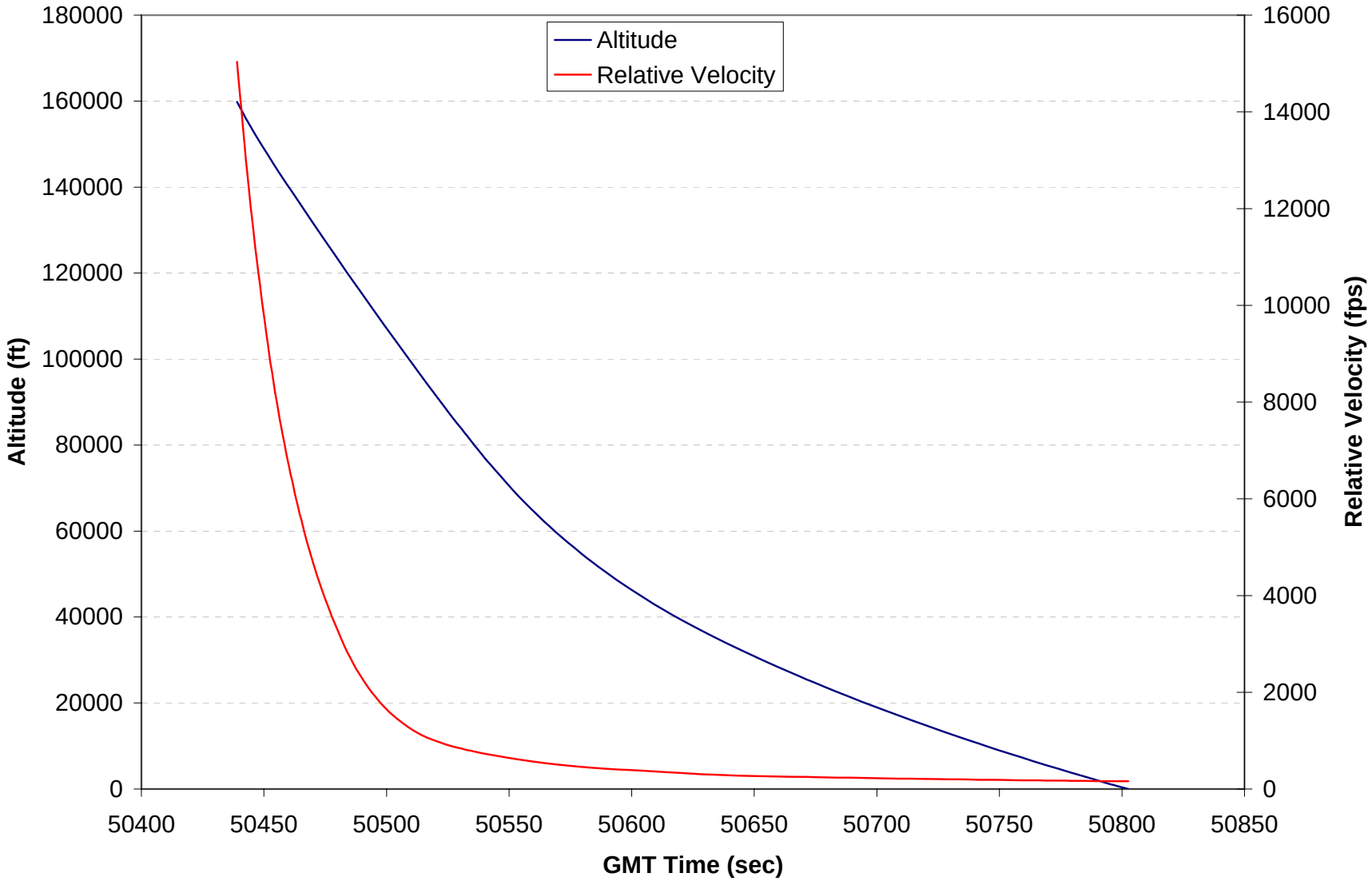

Figure 17: Reentry Altitude and Velocity Data for Debris #3 Method 4

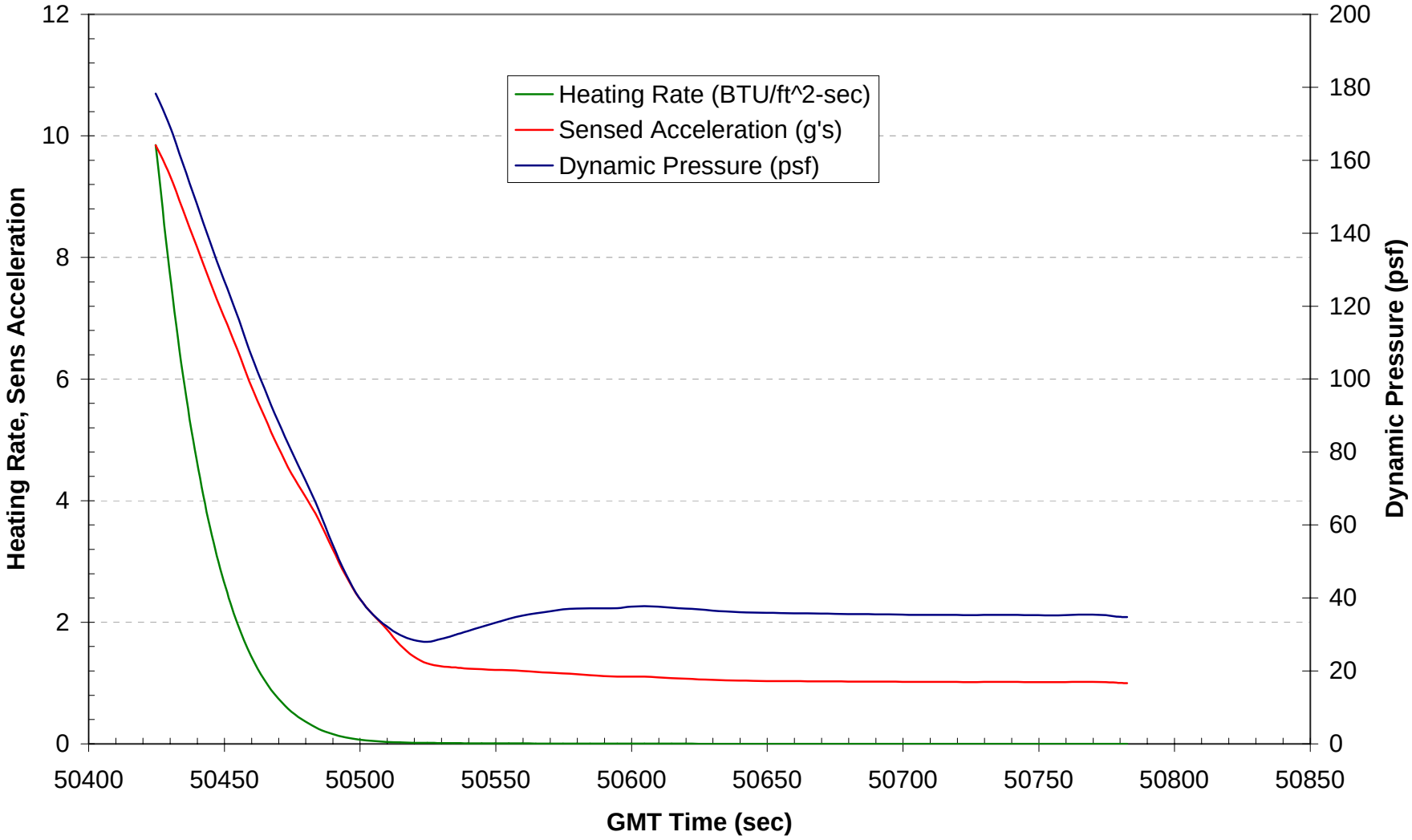

Figure 18: Reentry Heating and Loads Data for Debris #4 Method 4

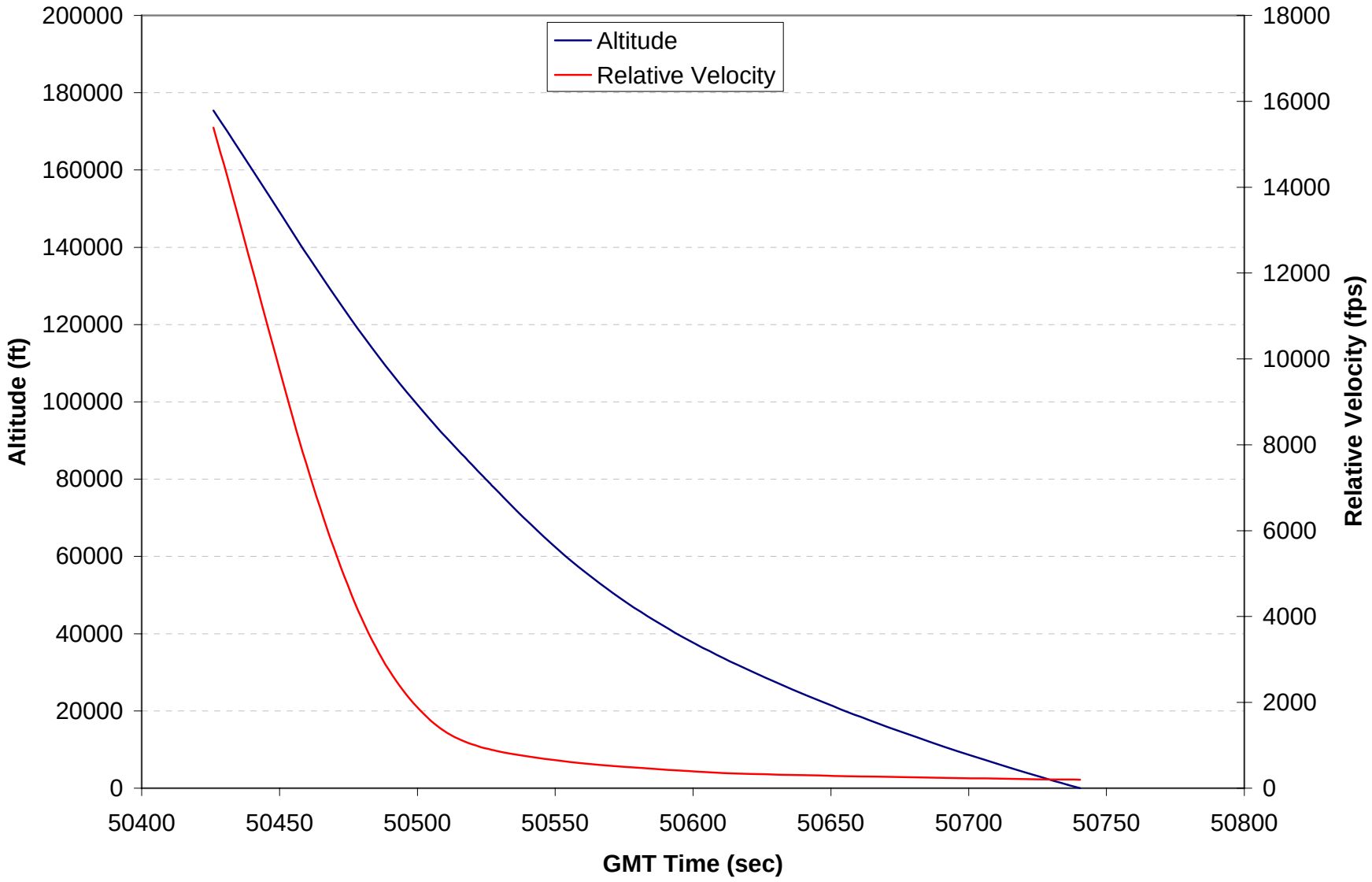

Figure 19: Reentry Altitude and Velocity Data for Debris #4 Method 4

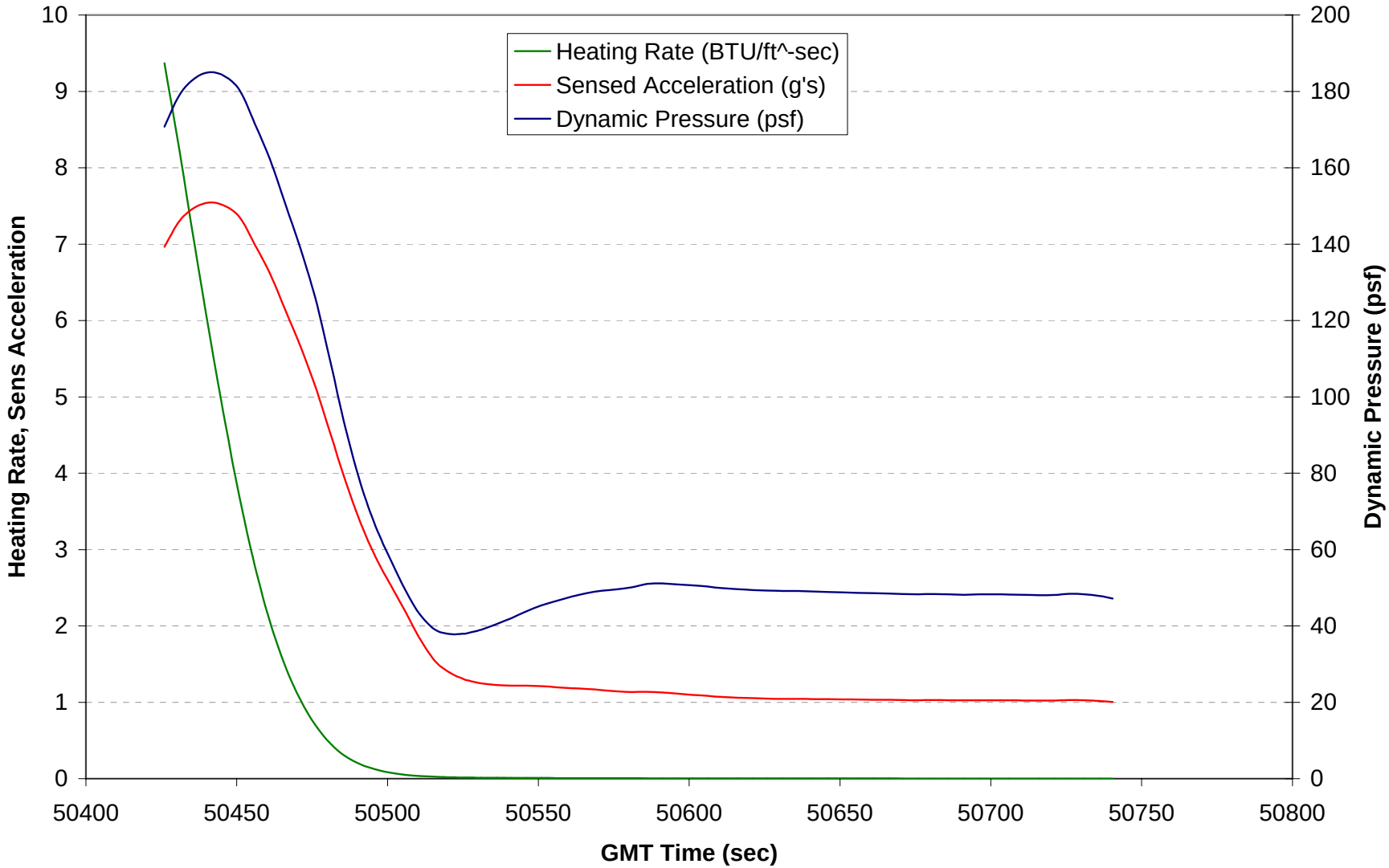

Figure 20: Reentry Heating and Loads Data for Debris #5 Method 4

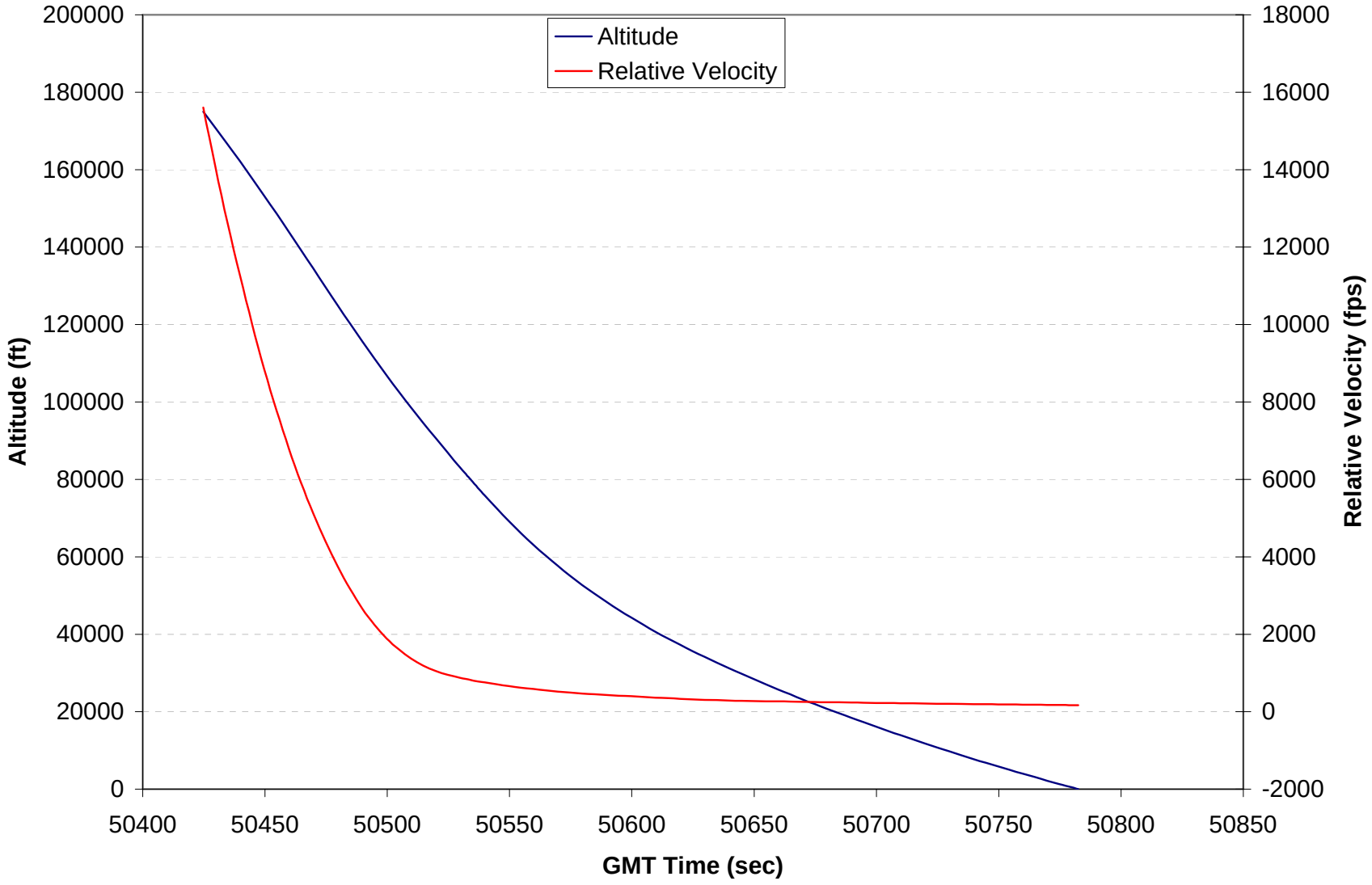

Figure 21: Reentry Altitude and Velocity Data for Debris #5 Method 4

Data available for $200 < T < 1500$ **K.**

Quadratic fit extrapolated to cover the range from absolute zero to 2000 K Air

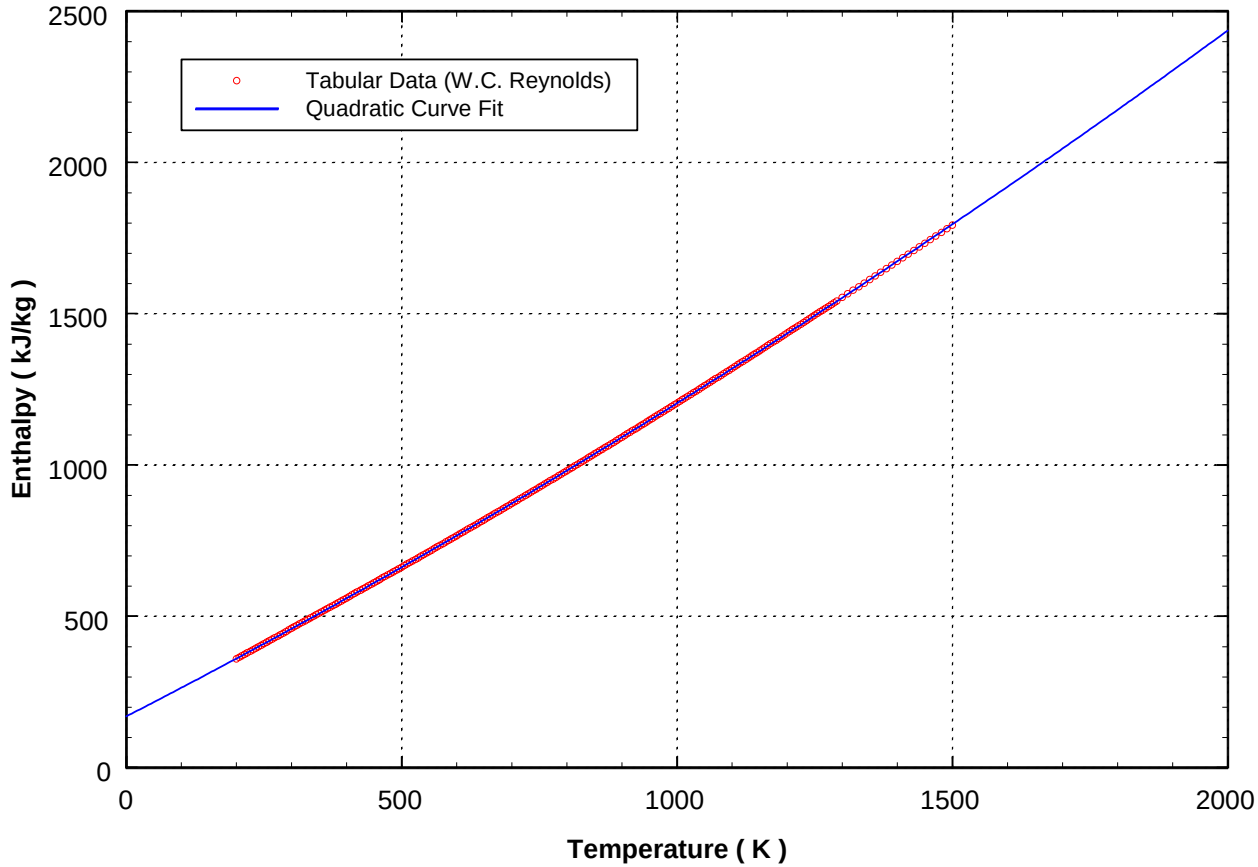

Figure 22: Enthalpy of Air

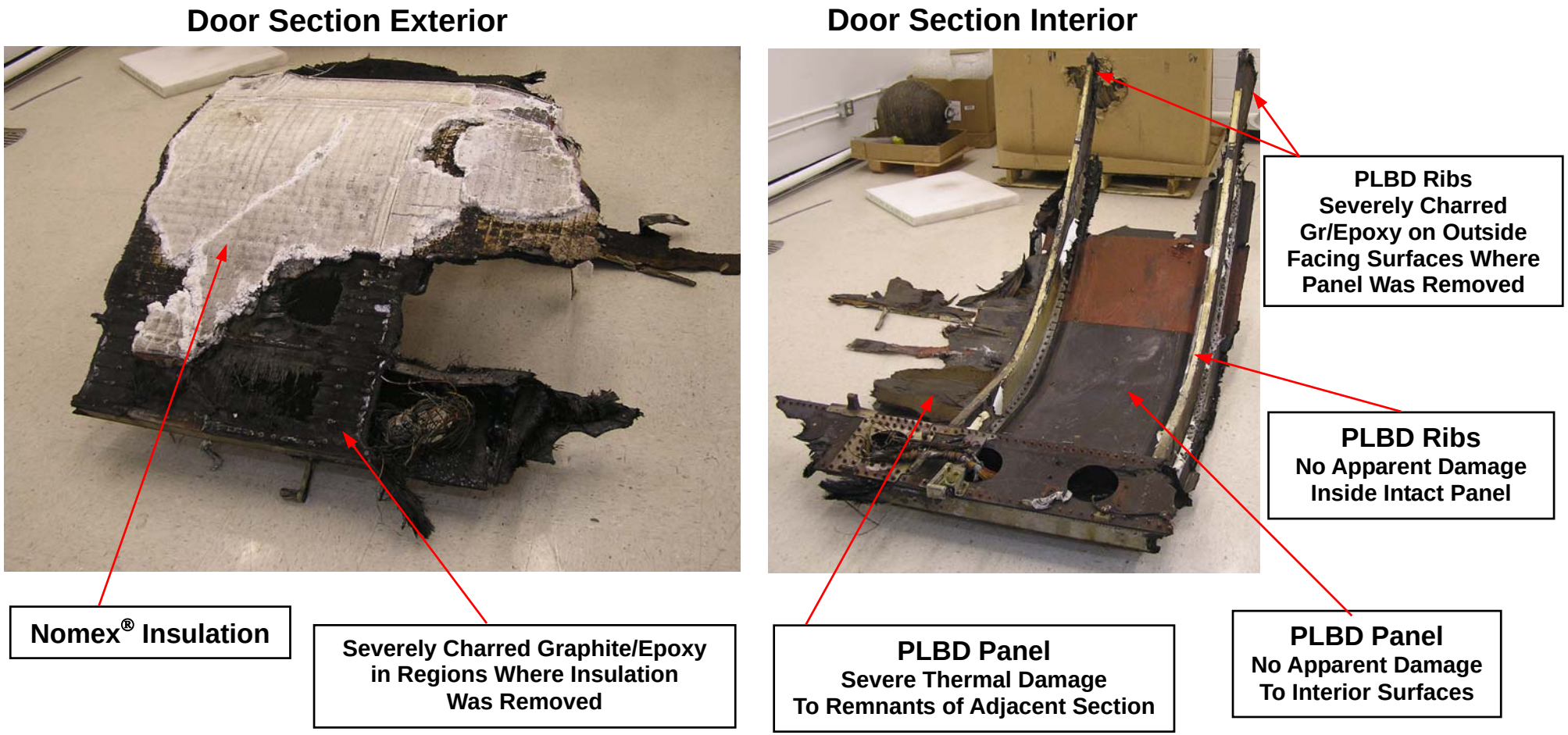

Figure 23: Payload Bay Door Exterior and Interior

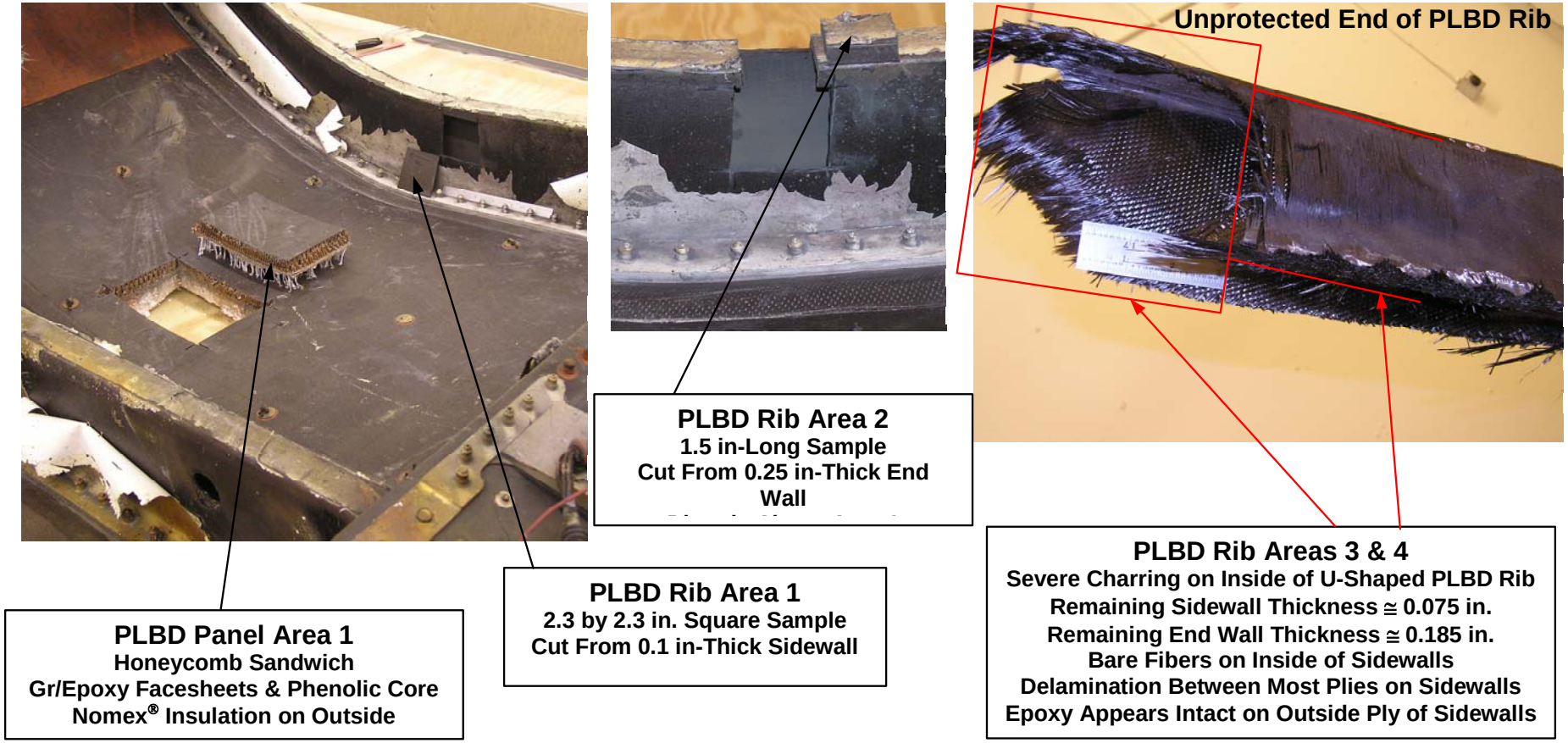

Figure 24: Payload Bay Door Sample Areas for Laboratory Analysis

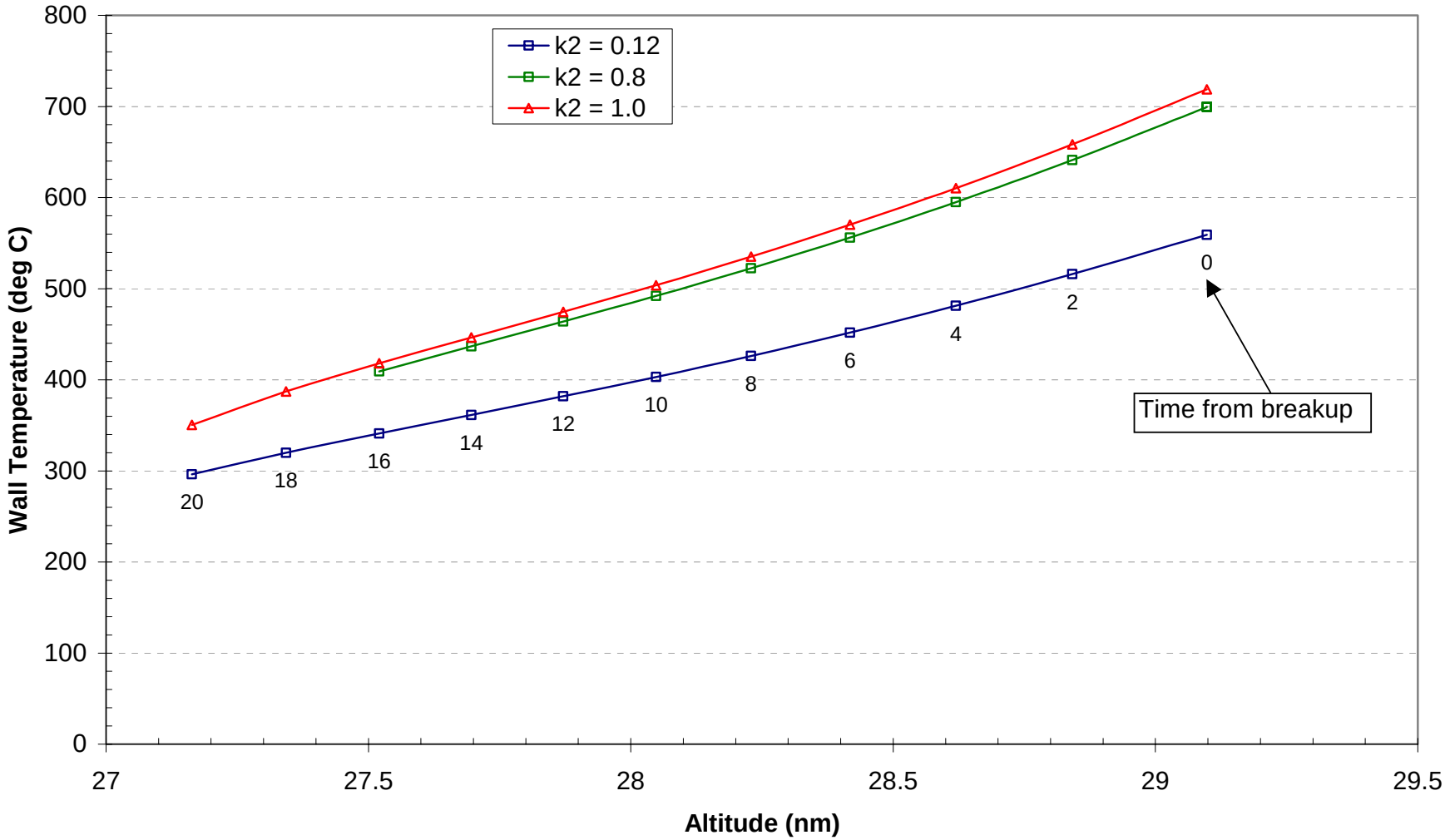

Figure 25: Predicted Wall Temperature for Payload Bay Door Area 4 with k_2 Varied

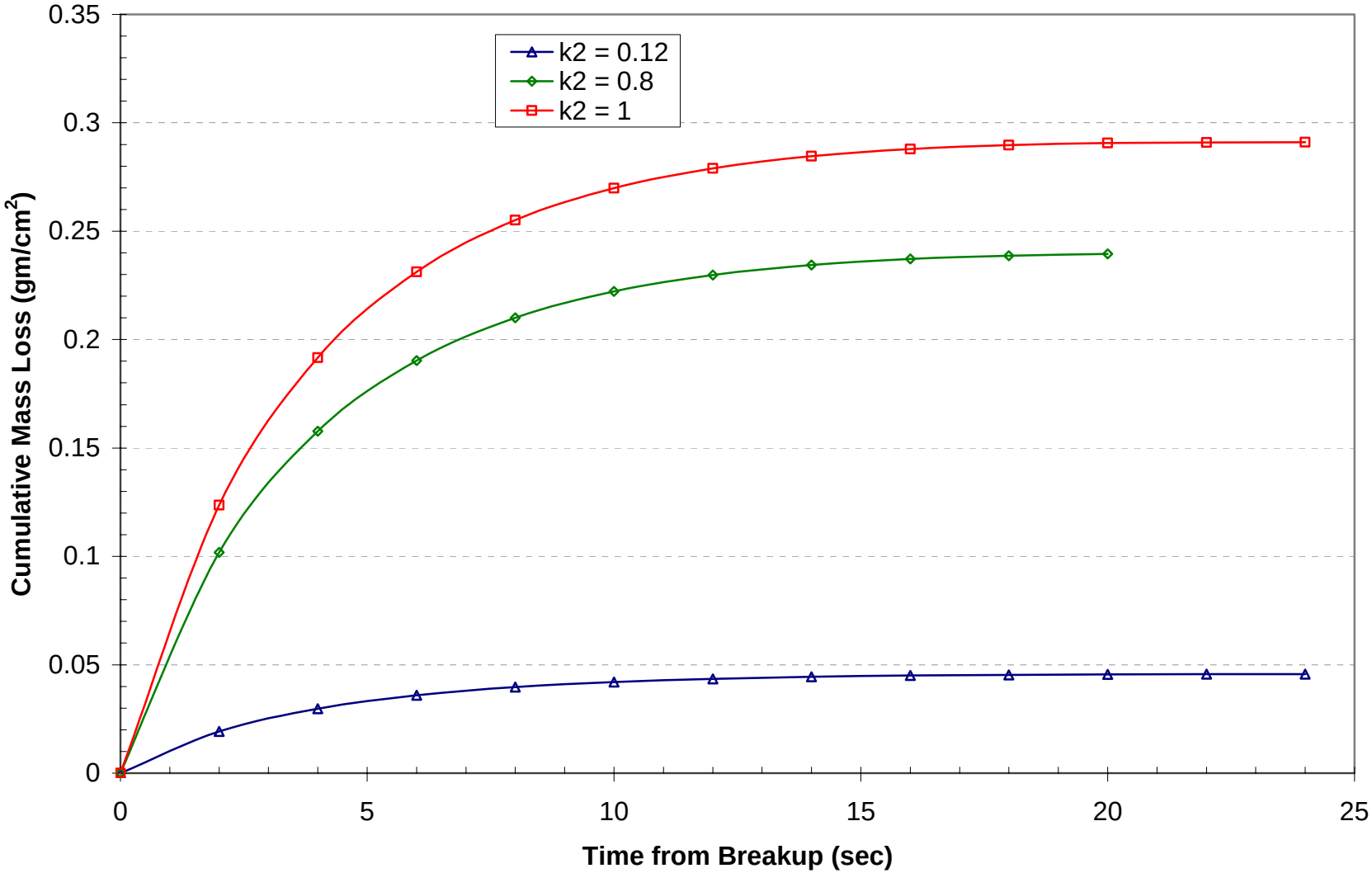

Figure 26: Predicted Cumulative Mass Loss for Payload Bay Door Area 4 with k_2 Varied

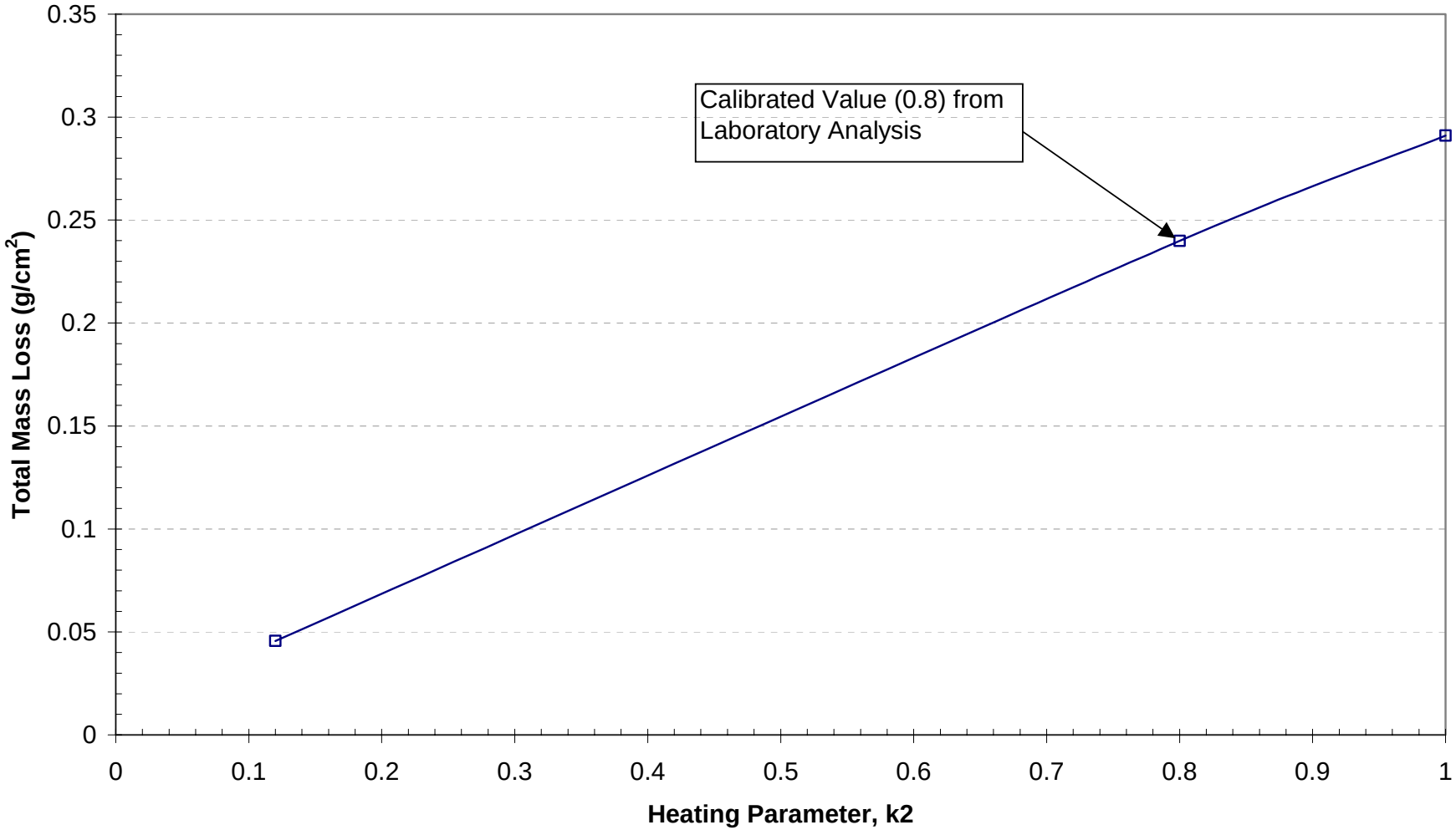

Figure 27: Predicted Payload Bay Door Area 4 Total Mass Loss with k_2 Varied

8. ABBREVIATIONS AND SYMBOLS

AST	Office of Commercial Space Transportation
B	frequency factor
BTU	British Thermal Unit
C_d	drag coefficient
C_l	lift coefficient
cm	centimeter
COTR	Contracting Officer's Technical Representative
deg	degree
DMA	Dynamic Mechanical Analysis
E	activation energy
FAA	Federal Aviation Administration
ft	foot
ft/sec	feet per second
gm	gram
h_{air}	enthalpy of air
h_b	base (cold) enthalpy of the epoxy resin
h_{py}	enthalpy of pyrolysis gas at wall
H^0	stagnation enthalpy of the external flow
k_2	area averaging heating factor
k_w	thermal conductivity of pyrolysis gas at wall
lb	pound
m	mass
M	Mach number
nm	nautical mile
PLBD	payload bay door
q	dynamic pressure
R	body radius
R	gas constant
R_{nose}	nose radius
ρB	atmospheric density
ρ_{sl}	atmospheric density at sea level
ρ_s	density of epoxy resin
s	second
S	aerodynamic surface area
TGA	Thermal Gravimetric Analysis
T_w	wall temperature of the ablating surface
v	earth relative velocity

REFERENCES

1. Hallman, W. P., Moody, D. M., Patera, R. P., and Stern, R. G., "Analysis of Videos of the STS-107 Reentry," Aerospace ATR-2003(7828)-3, 27 May 2003.

2. *Columbia* Accident Investigation Board Report Volume V, Appendix G.12, Crew Survivability, October 2003.

3. Fruth, G. and Shaw, M. A., "TOP 2.0a User Manual," Aerospace IOC # A2004-5447-4.007, 27 August 2004.

4. Moody, D. M., "Magnus Effect for Low-Speed Spinning Spheres," Aerospace IOC A2004-5447.4-029, 29 November 2004.

5. Moody, D. M., "Reentry Heating: Fundamental Concepts," Aerospace IOC A2001-5447.4-020, 10 July 2001.

6. Baker, R. L., "Outline of Approximate Graphite/Epoxy Ablation Model," 13 Jan 2005.

7. Reynolds, W. C., *Thermodynamic Properties in SI*, Stanford University, 1979.

8. Kemp, N. H., "Surface Recession Rate of an Ablating Polymer," AIAA J **6**, pp.1790-91, 1968.